

**Arjunolic acid modulate pancreatic dysfunction by ameliorating pattern recognition
receptor and canonical Wnt pathway activation in type 2 diabetic rats**

Khurram Aamir^{1,2}, Gautam Sethi³, Mst. Rejina Afrin⁴, Chowdhury Faiz Hossain⁴, Patricia
Regina Jusuf⁵, Satyajit D. Sarker⁶, Aditya Arya^{5,6,7}

¹*School of Pharmacy, Faculty of Health and Medical Sciences, Taylor's University, Subang Jaya, Malaysia*

²*Akhtar Saeed College of Pharmacy, Canal Campus, Lahore, Pakistan*

³*Department of Pharmacology, Yong Loo Lin School of Medicine, National University of Singapore, Singapore.*

⁴*Department of Pharmacy, Faculty of Sciences and Engineering, East West University, Dhaka, 1212, Bangladesh*

⁵*School of Biosciences, Faculty of Sciences, University of Melbourne, Parkville, VIC, Australia*

⁶*Centre for Natural Product Discovery, School of Pharmacy and Biomolecular Sciences, Liverpool John Moores
University, James Parsons Building, Byrom Street, Liverpool L3 3AF, United Kingdom*

⁷*Department of Pharmacology & Therapeutics, School of Medicine, Faculty of Health and Medical Sciences,
Taylor's University, Subang Jaya, Malaysia*

Corresponding Author:

Aditya Arya, PhD
Associate Professor
School of Bioscience
Faculty of Science
The University of Melbourne
Parkville, VIC
Tel: +610450080738
Email: aditya.arya@unimelb.edu.au

Abstract

Background: Arjunolic acid (AA) is a potent phytochemical with multiple therapeutics effects. In this study, AA is evaluated on type 2 diabetic (T2DM) rats to understand the mechanism of β -cell linkage with Toll-like receptor 4 (TLR-4) and canonical Wnt signaling. However, its role in modulating TLR-4 and canonical Wnt/ β -catenin crosstalk on insulin signaling remains unclear during T2DM. **Aim:** The current study is aimed to examine the potential role of AA on insulin signaling and TLR-4-Wnt crosstalk in the pancreas of type 2 diabetic rats. **Method:** Multiple methods were used to determine molecular cognizance of AA in T2DM rats, when treated with different dosage levels. Histopathological and histomorphometry analysis was conducted using masson trichrome and H&E stains. While, protein and mRNA expressions of TLR-4/Wnt and insulin signaling were assessed using automated Western blotting (jess), immunohistochemistry, and RT-PCR. **Results:** Histopathological findings revealed that AA had reversed back the T2DM-induced apoptosis and necrosis caused to rats pancreas. Molecular findings exhibited prominent effects of AA in downregulating the elevated level of TLR-4, MyD88, NF- κ B, p-JNK, and Wnt/ β -catenin by blocking TLR-4/MyD88 and canonical Wnt signaling in diabetic pancreas, while IRS-1, PI3K, and pAkt were all upregulated by altering the NF- κ B and β -catenin crosstalk during T2DM. **Conclusion:** Overall results, indicate that AA has potential to develop as an effective therapeutic in the treatment of T2DM associated meta-inflammation. However, future preclinical research at multiple dose level in a long-term chronic T2DM disease model is warranted to understand its clinical relevance in cardiometabolic disease.

Keywords, Arjunolic acid, Type 2 diabetes mellitus, TLR-4, Wnt, insulin signaling.

1. Introduction

Ageing is characterized by the gradual increase of low-grade inflammation, contributing to the incidence of chronic diseases and associated complications (George and Baker, 2016, Ottaviani et al. , 2012). Important factors that contribute to the onset of persistent low-grade inflammation is directly linked to the activation of innate immune receptors, the stimulation of immune cells, and the subsequent polymorphic alterations in the binding areas of numerous genes encoding pro-inflammatory cytokines (Frasca and Blomberg, 2016). In addition, a poor diet, irregular eating schedules, and a sedentary lifestyle plays an enormous role in the stimulation of innate immune receptors, which in turn triggers a form of inflammation called inflammaging. Obesity, cancer, atherosclerosis, and metabolic syndrome/diabetes are all linked to inflammaging, a prominent relationship between ageing and metabolic inflammation. Inflammaging is a condition where the innate immune system is triggered, setting up a chain reaction leading to an increase in pro-inflammatory cytokines. Insulin resistance and subsequent metabolic syndrome are surfaced by the interaction between inflammatory and insulin signaling (Hotamisligil, 2017). T2DM, a chronic metabolic condition is caused due to inadequate insulin production or poor sensitivity to insulin, either as a result of genetic predisposition or environmental factors (Almalki et al. , 2019). Hypertriglyceridemia, hyperglycemia, and the production of reactive oxygen species (ROS) are linked with T2DM caused by defective insulin function (Frasca et al. , 2017).

Moreover, excessive free fatty acids (FFA) production is due to the pancreatic failure and body organs switch from using glucose to FFA as their primary energy source (Nolan et al. , 2011). Consequently, excessive fatty acid metabolism increases pancreatic ROS generation and worsens oxidative stress (Singh et al. , 2022), that leads to activation of toll like receptors (TLRs), which then blocks insulin signaling and causes T2DM (Hameed et al. , 2015). TLRs are pattern recognition receptors (PRRs) which can trigger an inflammatory response in the

islets of Langerhans. Importantly, TLR-4 is particularly significant in the development of type 2 diabetes, by triggering FFA and ROS, which then stimulates myeloid differentiation factor 88 (MyD88), which in turn activates nuclear factor kappa-light chain enhancer of activated B cells (NF- κ B), kicking off an inflammatory response (Singh et al. , 2023). This situation further worsens by the recruitment of monocytes and macrophages by NF- κ B mediated pro-inflammatory cytokines; tumor necrosis factor alpha (TNF- α), interleukin 1 beta (IL-1 β) and mono-attractant protein 1 (MCP-1) (Yang et al. , 2016).

In addition to TLR4, Wnt signaling which is highly implicated in the regulation of physiological mechanisms such as cell migration, adhesion and differentiation are also involved in various chronic disorders including aging, cancer, diabetes and cardiometabolic disease (Arnold and Robertson, 2015). Canonical and non-canonical pathways have been identified in Wnt ligands and β -catenin as a sub-components of the canonical pathway, whereas the Wnt/Ca²⁺ and planar cell polarity (PCP) pathways are subsets of the non-canonical system (Aamir et al. , 2019b). Various findings suggest that T2DM is caused by the aberrant activation of either Wnt pathways or its differentiation cofactors which intersects and plays critical role in the TLR pathways (Ackers and Malgor, 2018). At this point, crosstalk between the TLR and Wnt pathway enhances the chances of proinflammatory cytokines release by further exacerbating metabolic inflammation. (Aamir et al., 2019b).

Phytochemicals and natural substances contain potential bio-chemicals of significant importance in the treatment and prevention of cardiometabolic diseases. However, compounds with potential therapeutic value are being extracted from plants prior to their testing on certain in-vivo disease models (Aamir et al. , 2019a). We have isolated AA from the bark of Combretaceae family tree; *Terminalia arjuna*, which has been used for ages in the Ayurvedic System of Medicine to treat cardiovascular diseases and its associated complications. In Ayurveda, “Arjunaristha” is a famous cardi tonic prepared from the bark of *Terminalia arjuna*

which helps to control the symptoms of heart disease and improve cardiac muscles functionality. Importantly, several bioactive compounds are abundantly found in the barks, such as flavonoids, tannins, phytosterols, and triterpenoid saponins. The triterpene saponins present in the *T. arjuna* bark includes; arjunic acid, arjungenin, arjunone, arjunolone and arjunolic acid (AA) (Facundo et al. , 2005, Ghosh et al. , 2010). Interestingly, arjunolic acid (2,3,23-trihydroxyolean-12-en-28-oic acid) exhibited diverse therapeutic potential on various preclinical approaches like, acute toxicity and preliminary screening on subacute T2DM rat model (Aamir et al. , 2022). However, current study is aimed to investigate the potential of AA in modulating pancreatic dysfunction and determine the linkage between pattern recognition receptor and the molecular mechanism involved in the canonical Wnt pathway activation and insulin resistance in type 2 diabetic rats.

2. Materials and Methods

Trichrome staining kit (ab150686, Abcam, Cambridge, UK), protein quantification kit (ab102536, Abcam, Cambridge, UK), Jess separation module (12-230 kDa) KIT (Protein Simple, SM-PN01-1), EZ standard pack (Protein Simple, PS.ST01EZ-8) containing biotinylated ladder, 5X fluorescent master mix, dithiothreitol (DTT), 10X sample buffer, antibody diluent, luminol-S, peroxide sample buffer, streptavidin HRP conjugate, wash buffer, protein normalization module, anti-rabbit and anti-mouse secondary antibodies were purchased from Protein Simple (San Jose, California, U.S.A).

Primary antibodies

Mouse monoclonal β -catenin (1:10 dilution, NBP1-54467, Novus Biologicals), rabbit monoclonal Wnt3a (1:10 dilution, ab210412, Abcam), mouse monoclonal PI3K (1:10 dilution, NBP2-67058, Novus Biologicals), mouse monoclonal cMyc (1:25 dilution, NB200-108, Novus Biologicals), rabbit polyclonal p-JNK1/2 (1:10 dilution, ab131499, Abcam), rabbit polyclonal IRS-1 (1:25 dilution, NB100-82001, Novus Biologicals), rabbit polyclonal p-

Akt1/2/3 (1:25 dilution, AF887, R&D), mouse monoclonal TLR-4 (1:10 dilution, NB100-56566, Novus Biologicals), mouse monoclonal NF- κ B (1:10 dilution, NB100-56712, Novus Biologicals), goat polyclonal MyD88 (1:25 dilution, AF3109, R&D), mouse monoclonal TNF- α (1:5 dilution, MAB510-100, R&D), mouse monoclonal MCP-1 (1:5 dilution, NBP2-22115, Novus Biologicals), mouse monoclonal IL-1 β (1:5 dilution, MAB5011-100, R&D), goat polyclonal notch1 (1:10 dilution, AF1057, R&D), rabbit polyclonal Dll4 (1:10 dilution, NB600-892, Novus Biologicals), rabbit polyclonal RBPJ- κ (1:5 dilution, NBP1-33427, Novus Biologicals), goat polyclonal IL-6 (1:5 dilution, AF506, R&D), rabbit monoclonal Hes-1 (1:10 dilution, NBP2-67642, Novus Biologicals), rabbit monoclonal p-GSK3 β (1:10 dilution, ab107166, Abcam), rabbit monoclonal p-IKK α/β (1:5 dilution, 2697, Cell Signaling), rabbit polyclonal Wnt2 (1:5 dilution, ab27794, Abcam) and rabbit polyclonal Wnt5a (1:10 dilution, ab235966, Abcam).

2.1 Experimental Design

The present work is the continuation of our previous study in which AA was isolated from the dried bark of *T. arjuna* and identified using NMR (Aamir et al., 2022). Briefly, thirty male Sprague Dawley rats of 8-10 weeks old with the average body weight of 250-300 grams were procured from the Animal Experimental Unit, Faculty of Medicine, University of Malaya, Kuala Lumpur, Malaysia. The facility was kept at 24°C, with a relative humidity of 50–60% and a 12-hour light/dark cycle. After arrival, all the animals had access to standard pellet diet and ad libitum. After one week acclimatization, T2DM was induced in 24 overnight fasted rats (80%) via single intraperitoneal (i.p) injection of 60 mg/kg STZ, after i.p administration of nicotinamide (120 mg/kg). All animals were divided into five groups containing 6 rats each (n=6). Group 1 served as non-diabetic control, while group 2 served as diabetic control. Whereas, Group 3 and 4 were orally administered with AA 25 and 50 mg/kg body weight respectively once in a day for 28 days and group 5 received metformin 250 mg/kg via oral

gavage. Later, all animals were euthanized under 35-50% carbon dioxide (Aamir et al., 2022). All the experiments were conducted upon approval from the Institutional Animal Care and Use Committee (IACUC) with Ethics No. 2019-210108/TAY/R/AA, Faculty of Medicine, University of Malaya.

2.2 Histopathological analysis

After euthanizing animals pancreas from diabetic and non-diabetic rats were carefully harvested and fixed in 10% formalin buffered solution. Later, pancreas were cut into small pieces and enclosed in cassettes, placed in 10% formalin (fixing) to start tissue processing. All steps of tissue processing was performed in a mechanical tissue processor (SLEE medical GmbH, SN: K13 0014, Mainz, Germany) and finally embedded in paraffin wax. Subsequently, embedded tissue sections were cut into 5 μ m using microtome (SLEE medical GmbH, SN: B 13 0010, Mainz, Germany). In order to reveal morphological changes in the architecture of the pancreas, hematoxylin and eosin (H&E) staining was performed using our previously described protocol (Aamir et al., 2019a). Further, to visualize collagen fiber deposition in the pancreas, a masson trichrome staining kit (ab150686, Abcam, Cambridge, UK) was used to stain tissue as per manufacturer's protocol (Aamir et al., 2019a, Clayton et al. , 2016, Khan et al. , 2020).

2.3 Histomorphometric analysis

To further elucidate the morphology of β -cells, histomorphometric analysis was performed on three different histological sections per slide from six animals. For this purpose, H&E-stained sections of pancreas were analyzed for counting and measuring islet number and size in 10 different, randomly selected microscopic fields by using ImageJ (1.52, National Institute of Health, USA). Before starting measurements, the software was calibrated for the conversion of measurement units (pixels) to millimeter (mm). The average number of islets from each selected field and their average size was computed for each group of rats. The result was

expressed as N/10 mm² of selected pancreatic fields as described previously. (Noor et al. , 2017). While, mean islets size was calculated from each group of animals after analyzing three different microscopic field as described by Mega and his colleagues (Mega et al. , 2014).

2.4 Automated Western Blot (Jess)

Automated western blot (jess) analysis was performed to highlight expression of selected protein targets in isolated pancreatic tissues from treated and non-treated rats. Tissue protein was extracted from the frozen pancreas by using 1X RIPA buffer (ab156034, Abcam, Cambridge, UK) followed by centrifugation at 15000 rpm at 4 °C for 15 min. Later, protein quantification was performed using bicinchoninic acid (BCA) kit (ab102536, Abcam, Cambridge, UK). Capillary jess analysis was performed according to predefined protocol on an automated “Jess system” (Protein Simple. JS-3076, San Jose, California, U.S.A). Initially, Jess standard reagents such as DTT, fluorescent master mix, biotinylated ladder, sample buffer, streptavidin HRP standards, separation matrix, running buffer, chemiluminescence substrates, normalization reagent, antibody diluents and wash buffers were prepared and used according to the manufacturer’s instructions. After dilution of tissue lysate with 0.1X sample buffer, sample was mixed with fluorescent master mix in the ratio of 4:1 with subsequent heating at 95 °C on heating plate for 5 min. Afterwards, antibodies were diluted with antibody diluent provided by Protein Simple. All primary antibodies were optimized to check the optimum dilution based on the information provided in the datasheet of individual antibodies and from the test run on jess equipment before starting original experiments. Finally, 3 µl of protein sample, prepared reagents, primary and secondary antibodies were dispensed into a delicate microplate with pre-defined layout. The plate was centrifuged at 2500 rpm at room temperature for 5 minutes. Filled microplate was installed into Jess equipment followed by several automated steps of electrophoretic separation as per default setting of the machine. At the end

of the operation, chemiluminescence was detected and quantified by the software Compass for simple western (SW), version 4.0.0.

2.5 Immunohistochemistry

To further support the jess analysis, immunohistochemistry (IHC) was carried out on the paraffin embedded pancreatic tissue sections from normal and treated groups to evaluate localization of target proteins using triple stain IHC kit (ab 183298, Abcam, Cambridge, UK). Primary antibodies including TLR-4 (1:2500), MyD88 (1:100), NF- κ B (1:100), p-JNK1/2 (1:1000), IRS-1 (1:25), Wnt3a (1:100) and β -catenin (1:200) were diluted and used to stain tissue specimen as per manufacturer's guidelines. Briefly, slides were baked on hot plate at 60 °C for 40 minutes followed by clearance in xylene and hydration in graded alcohol. Later, slides were heated in antigen retrieval solution pH 6 (S169984, DAKO, Denmark) in microwave (NN-ST25JB, Panasonic, Malaysia) at 100°C for 10 minutes and allowed to cool at room temperature. All slides were washed with Tris buffer saline tween 20 (TBST, S330630, DAKO, Denmark) and tissue specimens were encircled with DAKO pen (S200230, DAKO, Denmark). Following, 200 μ l hydrogen peroxide (H₂O₂) was applied to cover tissue for 10 min. After incubation with H₂O₂, diluted primary antibody (200 μ l/slide) was applied and incubated overnight at 4 °C and next day, all slides were washed with TBST. For primary antibodies of mouse origin, mouse primer was applied to the slides for 10 minutes, followed by mouse HRP polymer for 30 minutes of incubation, while for rabbit origin antibodies, rabbit HRP polymer was added directly for 15 min. Again, slides were washed with TBST and 3,3'-diaminobenzidine (DAB) was applied for 5-10 min. Afterwards, distilled water was added on all slides to stop the reaction and counterstain in hematoxylin followed by rinsing in acid alcohol for differentiation (30 sec) and air dried with dryer. Lastly, all slides were rehydrated and cleared in graded alcohol and xylene respectively, and mounted with dibutylphthalate

polystyrene xylene (DPX) mounting media and observed under a microscope (Eclipse Ni-U, Nikon Corporation, Tokyo, Japan).

2.6 Real-time PCR

Expression of genes were analyzed to investigate the selected target mRNA at the transcriptional level. The whole experiment was divided into three steps comprising of mRNA isolation, cDNA strand synthesis and real time PCR analysis for the assessment of gene of interest. After harvesting, section of pancreas was kept in RNA Later solution (Cat No. 76104, Qiagen, Hilden, Germany) and directly stored at -80°C for further use. Total RNA was isolated from pancreas using RNeasy plus Mini Kit (Qiagen, Hilden, Germany) according to manufacturer protocol. Quantification of isolated RNA was determined via 260/280 UV absorption ratios (Gene Quant 1300, GE Healthcare UK Limited, Buckinghamshire, UK). After quantification, 1µg of total RNA was reverse transcribed to complementary DNA (cDNA) using high capacity RNA to cDNA kit (Applied Biosystems, Foster City, CA, USA). Real-time PCR was performed on the Realplex² Mastercycler (Eppendorf, USA) PCR system using Taqman probe as per manufacturer guidelines. Briefly, pre-incubation and pre-denaturation at 95 °C for 10 min, denaturation at 95 °C for 5 s, annealing at 60 °C for 30 s and extension at 72 °C for 30s followed by amplification of polymerase chain reaction with total 40 cycles. In order to determine, the relative expression of the target gene, glyceraldehyde 3-phosphate dehydrogenase (GAPDH) was used as an internal control. The gene expression was quantified by $2^{-\Delta\Delta C_t}$ method.

2.7 Statistical analysis

Results were expressed as the mean \pm standard deviation (SD). Normality of the data was analyzed by Kolmogorov-Smirnov and Shapiro-Wilk test. The statistical variations between groups were analyzed using one-way analysis of variance (ANOVA) followed by Tukey's

range test using GraphPad Prism 8 version 8.3.1 (San Diego, CA, U.S.A). Differences were considered significant at ($p < 0.05$).

3. Results

3.1 AA attenuated pancreatic degenerative changes during T2DM

Histopathological examination of H&E stained pancreas from non-diabetic animals demonstrated regular morphology. We observed, well defined circular or oval shaped islets of Langerhans in the pale stained area, bordered by the darkly stained pancreatic acini. The islets were organized in a cord-like structure, branched and anastomose with intertwining blood vessels. While, exocrine portion showed normal histoarchitecture characterized by closely arranged acini lined with pyramidal cells (Figure 1A).

Streptozotocin triggered multiple degenerative alterations to the islets of Langerhans and leads to cell apoptosis and necrosis, including islet shrinkage and karyolysis. Some islets were skewed with vacuolated cytoplasm, smaller and darkly stained nuclei with congested blood capillaries. Exocrine portion exhibited distorted acini with derangement of pyramidal cells (Figure 1B). AA (25 and 50 mg/kg) and metformin (250 mg/kg) significantly reduced islet degeneration during T2DM. Although, darkly stained pyknotic nuclei and vacuolated cytoplasm were visible with 25 mg/kg of AA (Figure 1C), however, treatment with AA 50 mg/kg and metformin significantly attenuated these effects. Moreover, the pancreatic acinar cells were typically arranged as shown in figure 1D and E.

Conversely, masson trichrome staining of pancreas sections from normal rats showed typical architecture, characterized by regular arrangement of alpha and beta cells surrounded by a densely stained zone of tightly packed well-organized pancreatic acini (Figure 2A). Nevertheless, extensive deposition of collagen fiber around pancreatic acini and in the area surrounding of islets showed fibrotic signature associated with STZ-mediated injury in the

diabetic rats. Similarly, islets with karyolysis and distorted acinar cells were also observed (Figure 2B). However, both the dosage of AA and metformin (250 mg/kg) treatment reduced deposition of collagen and regular outline was exhibited by acinar and islets cells, as compared to non-treated diabetic control (Figure 2C, D and E).

3.2 Islets morphometric analysis

Multiple degenerative alterations in islets of Langerhans were induced by STZ. Therefore, quantity and size of islets were drastically diminished in untreated diabetic rats as shown in Figure 3B. Moreover, distorted shape of islets was evident in non-treated diabetic animals compared to normal rats. Treatment with 25 and 50 mg/kg of AA and metformin (250 mg/kg) demonstrated marked improvement in the size and number of islets. Furthermore, the acinar cells in the pancreas section of treated groups restored their normal shape as shown in figure 3.

3.3 Automated Western Blot (Jess)

3.3.1 AA downregulated TLR-4/MyD88 pathway in pancreas

To evaluate markers of meta-inflammation, jess was used to investigate the inflammatory cascade in the pancreas by examining the expression of selected protein targets from the TLR-4/MyD88 pathway. TLR-4 expression was higher in the pancreas of untreated diabetic rats, as compared to normal control, although not statistically significant ($p>0.05$). Likewise, the expression of TLR-4 was not significantly lowered by AA (25 and 50 mg/kg) and metformin when compared with untreated diabetic rats ($p>0.05$) as shown in Figure 4. Then, we further investigated expression of TLR-4 adaptor protein and MyD88. Interestingly, we observed significant increase in the expression of MyD88 in diabetic control vs normal control ($p<0.005$). However, MyD88 expression was observed to be considerably decreased by AA 50 mg/kg ($p<0.001$) and metformin ($p<0.05$), but the expression was non-significantly

reduced by AA 25 mg/kg as compared to DC ($p>0.05$) (Figure 5). To further reveal the activation of downstream target of MyD88, phospho-IKK α/β and NF- κ B were investigated. Unfortunately, no expression for p-IKK α/β could be observed, however, NF- κ B expression was found to be upregulated in non-treated diabetic control as compared to normal rats ($p<0.005$). Administration of 25 and 50 mg/kg of AA and metformin substantially reduced expression of NF- κ B, as compared to diabetic control ($p<0.005$) as shown in Figure 6. These results are in consistent with our previous findings in which level of proinflammatory cytokines including TNF- α , IL-1 β and IL-6 was raised due to elevated expression of NF- κ B (Aamir et al., 2022).

3.3.2 AA ameliorated JNK mediated defective insulin signaling in pancreas

A major contributor to T2DM is a malfunction in the insulin signaling pathway. Due to apoptosis and necrosis of islet cells, insulin signaling was attenuated in the present STZ-induced diabetes model. On the molecular ground, these events are associated with JNK activation which leads to the development of insulin resistance (Feng et al. , 2020). Therefore, the expression of p-JNK1/2 was studied in the pancreatic lysate of normal and treated diabetic rats. Interestingly, significantly elevated expression of p-JNK1/2 was observed in DC vs NC ($p<0.001$). Although, treatment with AA (25 and 50 mg/kg) and metformin significantly reduced the expression of p-JNK1/2 as compared to DC ($p<0.05$) (Figure 7).

Mechanistically, activated JNK1/2 phosphorylates serine residue of IRS-1 and inhibits insulin signaling in the β -cells (Yung and Giacca, 2020). Hence, we analyzed pancreatic lysate for IRS-1 protein expression along with PI3K and p-Akt 1/2/3, two downstream targets of insulin signaling. The blots showed significant downregulation of IRS-1 ($p<0.0001$), PI3K ($p<0.005$) and p-Akt 1/2/3 ($p<0.05$) in non-treated diabetic control vs NC. Treatment with AA (25 and 50 mg/kg) and metformin increased expression of insulin signaling proteins, although

this effect was not statistically significant when compared with DC ($p>0.05$) presented in Figures 8-10.

3.3.3 Effect of AA on Wnt/ β -catenin signaling in pancreas

In order to confirm the crosstalk between the TLR-4-NF- κ B axis and the components of canonical Wnt pathway including Wnt3a and its downstream targets, β -catenin and c-Myc were studied in the pancreas T2DM rats. Remarkably, upregulated expression of Wnt3a ($p<0.001$), β -catenin ($p<0.005$) and c-Myc ($p<0.05$) were noted in untreated diabetic group as compared to non-diabetic rats. T2DM linked elevated expression of Wnt3a was substantially suppressed by AA (25 and 50 mg/kg) and metformin ($p<0.001$) shown in figure 11. Similarly, immediate effector of Wnt3a, β -catenin expression was also significantly downregulated by 25 and 50 mg/kg AA ($p<0.05$) but not with metformin ($p>0.05$) vs DC (Figure 12). Whereas, c-Myc expression was also downregulated by AA (25 and 50 mg/kg) and metformin, but the difference was not statistically significant compared to DC ($p>0.05$) (Figure 13).

3.4 Immunohistochemical observations

Immunohistochemical analysis was used to investigate the localization of TLR-4, MyD88, NF- κ B, p-JNK1/2, IRS-1, Wnt3a and β -catenin in the islets of Langerhans. All the selected targets were expressed and distributed normally in non-diabetic rats. Conversely, non-treated diabetic rats exhibited increased expression of TLR-4, MyD88, NF- κ B, p-JNK1/2, Wnt3a, and β -catenin, while IRS-1 expression was nearly undetectable ($p<0.05$). TLR-4 (Figure 15), MyD88 (Figure 16) and NF- κ B (Figure 17) expressions were significantly high in non-treated diabetic rats. The expression and distribution of TLR-4 and NF- κ B were greatly reduced after treatment with AA at 25 and 50 mg/kg ($p<0.0001$), whereas expression of MyD88 was reduced non-substantially with AA. Likewise, immunostaining showed that p-JNK1/2 was considerably overexpressed in diabetic rats compared to normal control ($p<0.0001$) presented

in Figure 18. However, AA treated groups (25 and 50 mg/kg) demonstrated drastic decrease in the p-JNK1/2 localization in the pancreas ($p<0.0001$). Conversely, distribution of IRS-1 was significantly diminished in the islets of diabetic animals ($p<0.0001$) (Figure 19). But the expression of IRS-1 was considerably increased in diabetic rats given AA 50 mg/kg and metformin when compared to non-treated diabetic animals ($p<0.05$). However, high distribution of Wnt3a and β -catenin was noticed in the pancreatic sections of T2DM rats ($p<0.0001$) as compared to normal littermates. Interestingly, the increased expression of Wnt3a/ β -catenin was dramatically decreased in diabetic rats treated with AA and metformin ($p<0.05$) as shown in the Figures 20 and 21.

3.6 AA downregulated mRNA expression of TLR-4, Wnt and insulin pathway

The trend in mRNA expression of TLR-4/MyD88 pathway is similar to that observed in the protein expression in the pancreas. T2DM was associated with markedly increased gene expression of TLR-4, MyD88, and NF- κ B ($p<0.05$) vs normal rats. Likewise, mRNA expression of pro-inflammatory cytokines such as TNF- α and IL-1 β were significantly increased in DC vs NC ($p<0.05$). Consequently, elevated mRNA transcripts of cytokines significantly downregulated expression of IRS-1 at transcriptional level in the pancreas of diabetic rats indicating suppression of insulin signaling ($p<0.05$) as shown in figure 22. Gene expression of TLR-4 was downregulated, but not considerably ($p>0.05$) following 28 days of treatment with 25 and 50 mg/kg of AA and metformin, while mRNA expression of MyD88 and NF- κ B was markedly downregulated ($p<0.05$). These results are in line with our protein expression analysis. Similarly, mRNA expression of TNF- α and IL-1 β was also substantially decreased by 50 mg/kg AA and metformin but not with 25 mg/kg of AA ($p>0.05$) as compared to DC ($p<0.05$). However, gene expression of IRS-1 was upregulated non-significantly by AA (25 and 50 mg/kg) and metformin ($p>0.05$) vs DC (Figure 22).

In contrast, Wnt3a, β -catenin, and c-Myc transcripts were markedly higher in untreated diabetic rats compared to normal control animals ($p<0.05$). The increased gene expression of Wnt3a was significantly decreased ($p<0.05$) in 50 mg/kg of AA and metformin treated groups. On the other hand, elevated mRNA expression of β -catenin in diabetic rats was considerably decreased by AA (25 and 50 mg/kg) and metformin ($p<0.05$). Whereas, c-Myc transcript was not considerably altered by AA (25 and 50 mg/kg) and metformin when compared to DC ($p>0.05$) (figure 22).

4. Discussion

The prevalence of diabetes and the consequences that arise from insulin resistance is a common effect of uncontrolled diabetes and over time leads to serious damage to many of the body's systems, especially the nerves and blood vessels (Aamir et al., 2019b). The current findings expand on preceding investigations and stipulate a crosstalk between TLR-4-Wnt axis which has a negative impact on insulin signaling in pancreatic tissues of T2DM rats. The pleiotropic factors NF- κ B and β -catenin are stabilized after being recruited to the membrane following aberrant activation of TLR-4, Wnt, and Notch pathways affecting pancreatic cells and leading to development of T2DM (Aamir et al. , 2020). In the current study, an in-depth investigation is performed at the molecular level on pancreatic tissues to assess how AA acted on various targeted signaling proteins and revealed some interesting insight on the selected signaling pathways to flame the fire of meta-inflammation.

Pathogenesis of T2DM is heavily reliant on chronic low-grade inflammation, which is carried out by pro-inflammatory cytokines, whereas, insulin resistance, develops as a response to metabolic inflammation (Cam et al. , 2019). After analyzing the biochemical parameters (Aamir et al. , 2021), we further proceeded to assess the histoarchitecture of the pancreas. We observed the structural degradation and collagen deposition in the exocrine portion and the islets of Langerhans were seen in H&E and masson trichrome stained sections of pancreas

obtained from untreated diabetic control rats (Figures 1 and 2). Several mechanisms have been proposed to elucidate pancreatic damage in the setting of T2DM. These pathological mechanisms comprise of metabolic stress mediated activation of inflammatory pathways, which further accelerate oxidative and endoplasmic reticulum stress (Halban et al. , 2014). In morphometric analysis diabetic rats have exhibited significant decrease in number of islet cells and the size, compared to normal rats, which is in line with the histopathological findings (Figure 3). It is to be noted that, rate of insulin secretion are relatively expressed to islet insulin content, which is dependent of differences in the size and number of islet cells (Aamir et al., 2021). Moreover, masson trichrome staining of diabetic control specimens showed aberrant deposition of collagen surrounding pancreatic acini and islets, highlighting fibrotic hallmark due to activation of inflammatory pathways (Figure 2). Similar results was observed by Zhou and Hussien in the rats pancreas after STZ-NIC treatment (Hussien et al. , 2017, Zhou et al. , 2013). Interestingly, as a result of AA treatment, the morphology of islet cells was significantly improved in the number and size, including aberrant collagen stroma in the pancreas (Figure 3).

Streptozotocin destruct pancreatic β -cells and increases oxidative stress, disruption of lipid metabolism, hyperglycemia, and excess FFA generation due to insulin insufficiency, which results in reactive oxygen (ROS) and reactive nitrogen species (RNS). In addition, STZ also liberates nitric oxide (NO) during its metabolism in β -cells and increases expression of pro-inflammatory cytokines (Manna et al. , 2010). Disturbances in glucose metabolism, FFA and ROS generation is the hallmark of T2DM and serves as an internal ligand for the activation of PRR or TLR. However, the TLR family of receptors are important for both the innate immune system and act as the major cause of inflammation in an advert condition. TLR-4 is basically a pattern recognition receptor, its overexpression in the pancreas of diabetics is associated with

437 MyD88 and NF- κ B activation and a consequent elevation of pro-inflammatory cytokines that
438 leads to deactivation of the innate immune system.

439 However, results from various preclinical findings and computational simulation have
440 demonstrated that phytochemicals and natural products have an ability to target TLR4 which
441 blocks the TLR4-nuclear factor-kappa B (NF- κ B) pathway and reduces the inflammatory
442 response and complications associated with T2DM (Baffy, 2009, Li et al. , 2012, Shi et al. ,
443 2006). Our current findings have demonstrated that administration of AA (25 and 50 mg/kg)
444 inhibited MyD88-dependent TLR-4 signaling pathway. In line with this, immunohistochemical
445 examination provides further support for our findings by decrease in the widespread
446 distribution of TLR-4, MyD88, and NF- κ B in diabetic rats. Based on these data, we postulated
447 that the TLR-4/MyD88/NF- κ B axis might have significant role in metabolic inflammation
448 during type 2 diabetes. The anti-inflammatory activity of AA are in line with the earlier
449 research, which showed that *Averrhoa carambola* roots reduced TLR-4/NF- κ B-mediated
450 inflammation in the pancreas of STZ-induced diabetic rats (Xu et al. , 2015).

451 Next, we explored TLR-4-mediated insulin resistance in the pancreas of T2DM rats.
452 Various findings have shown that TLR-4/MyD88 mediated NF- κ B activation increases pro-
453 inflammatory cytokines such TNF- α and IL-1 β , these cytokines are crucial contributors to
454 insulin resistance and β -cell dysfunction (Aamir et al., 2021) (Guilherme et al. , 2019).
455 Pancreatic insulin signaling is disrupted at the molecular level by the activation of
456 serine/threonine kinases by cytokines such c-Jun NH₂-terminal kinase (JNK) and inhibitor of
457 nuclear factor- κ B. In a healthy organism, JNK1/2 are involved in the stress response
458 mechanism by contributing to β -cell differentiation and proliferation.

459 However, FFA and pro-inflammatory cytokines continuously phosphorylate JNK1/2
460 (active state), resulting in β -cell dysfunction (Lanuz-Masdeu et al. , 2013, Yung and Giacca,

2020). Due to increased serine phosphorylation by p-JNK1/2, insulin receptor substrate 1 (IRS-1) activation was blocked. Inhibition of IRS-1 hampers activation of downstream PI3K and p-Akt proteins and further reduced p-Akt activity and overexpressed p-JNK1/2 enhanced nuclear translocation of forkhead box protein O1 (FOXO1) to inhibit insulin gene transcription (Yung and Giacca, 2020). Our results have shown that the treatment of AA had reversed back the downregulated IRS-1, PI3K, and p-Akt1/2/3 in T2DM animals via p-JNK1/2. Interestingly, these results are in agreement with the immunohistochemical examination of pancreatic sections which demonstrated similar results in normal and AA-treated rats. Previous findings by Manna and colleagues (Manna and Sil, 2012) showed AA reduced JNK expression in the spleen and renal tissues of murine model of type 1 diabetes. Taken together, our findings suggest that AA might have immunomodulatory effects which reduced metaflammation and insulin resistant states in T2DM.

Moreover, the Wnt/ β -catenin pathway has been shown to play a significant role in preserving β -cell function. According to the study conducted by Sorrenson et al. (2016), β -catenin plays an important role in increasing insulin release from β -cells and it is well established that canonical Wnt signaling is responsible for the development of pancreas (Scheibner et al. , 2019). However, at the same time there are evidences which support the opposite impact of Wnt/ β -catenin pathway in provoking T2DM (Nie et al. , 2021). Although, Wnt/ β -catenin activation in the pancreas has been well-documented, its precise involvement in the pancreas during metabolic syndrome remains a mystery. To reveal this fact, we have examined the crosstalk between the canonical Wnt/ β -catenin pathway and the TLR-4 signaling in the pancreas. In this finding, we observed overexpression of Wnt3a in the pancreatic lysate of untreated diabetic rats, when compared to normal animals (Figure 11). Notably, upregulation of Wnt3a is essential to indicate the presence of ligand in activating the pathways.

Next, the activation of soluble Wnt in the islets was validated by the overexpression of stabilized β -catenin by Wnt3a in non-treated diabetic pancreas (Figure 12). Remarkable activation of β -catenin in this setting might relate to diabetes through the mechanism involving insulin-mediated regulation of p-GSK3 β via the PI3K/Akt pathway (Cross et al. , 1995). This suggests that hyperinsulinemia, a hallmark of STZ-NIC-induced T2DM, may result in an increased level of β -catenin, a site of interaction with insulin signaling. Unfortunately, expression of p-GSK3 β was not detected in the pancreatic lysate of treated and non-treated rats. Activation of Wnt/ β -catenin pathway also raised an important question, whether this activation is an adaptive response or pathologic response during type 2 diabetes. Possibly, this might be due to the canonical Wnt activation, an adaptive response in early stages of T2DM to enhance β -cell proliferation.

However, it has another side to consider, chronic activation causes cell death, a well-established role of c-Myc, an effector protein of canonical Wnt signaling. Previous findings on transgenic mouse model of diabetes, c-Myc had emerged as a strong candidate as an inducer of β -cell death (Radziszewska et al. , 2009). High levels of c-Myc expression were observed in the pancreas of untreated diabetics (Figure 13), correlating with the decreased number of islet cells, observed by histomorphometric analysis. Intriguingly, metabolic inflammation is also exacerbated by interaction between Wnt/ β -catenin and NF- κ B. The TNF- α produced by the TLR-4/NF- κ B axis may inactivate GSK3 β to boost β -catenin level, which in turn increases c-Myc expression (Ma and Hottiger, 2016). In consistent with the previous research, our data demonstrated that Wnt3a/ β -catenin activation in the pancreas has a detrimental role in T2DM. Interestingly, diabetic rats treated with AA for four weeks, reduced canonical Wnt activity by demonstrating its critical role in diabetic conditions. In addition, immunostaining revealed the same pattern, including the widespread distribution of Wnt3a/ β -catenin, in diabetic rats.

Although, these expression levels were decreased gradually after AA administration (Figure 20 and 21). Taken together, AA exhibited anti-inflammatory, antidiabetic effects by modulating TLR-4/Wnt/ β -catenin signaling in the pancreas.

In line with an evolutionary conserved signaling pathways, we examined the functionality of Notch signaling, which is responsible for maintaining islets cell homeostasis. Its persistent activation was seen in β -cells during T2DM, which is responsible for impairing glucose stimulated insulin secretion from islets of Langerhans (Bartolome et al. , 2019, Billiard et al. , 2018). Considering the fact, we studied Notch1, delta like ligand 4 (Dll4, Notch ligand) and its downstream adapter protein, recombination signal binding protein for immunoglobulin kappa J region (RBP-J κ) and hairy enhancer of split 1 (Hes 1). However, we did not find any expression pertaining to the Notch signaling protein via automated jess analysis in pancreatic lysates of T2DM rats.

Recent progress in RNA-mediated changes during T2DM and accompanying complications raised the need to investigate mRNA expressions of several protein targets. It is also well-established that one gene can synthesize many proteins by the use of short non-coding RNAs (snRNAs) and other transcriptional components which generate wide variety of mRNAs in complex three-dimensional structures (Aamir and Arya, 2023, Marchese et al. , 2016). Therefore, mRNA expression of selected protein targets is investigated and we observed that the expression of the TLR-4, MyD88 and NF- κ B genes were upregulated in the untreated diabetic animals (Figure 22), which is in agreement with the protein expressions examined via jess (western blot) analysis. The mRNA expression of TNF- α and IL-1 β were also upregulated, as compared to normal rats, highlighting activation of MyD88 dependent TLR-4 signaling at transcriptional level. Effectively, AA had suppressed the selected gene transcriptions in the diabetic rats. Conversely, AA administration downregulated the elevated level of Wnt3a, β -

catenin and c-Myc mRNA expression in diabetic rats. These outcomes resemble most of the protein expression observed during Jess analysis and correlate the crosstalk between TLR-4/Wnt pathway at the transcription level, which is essentially downregulated with the treatment of AA. On the other hand, IRS-1 was also upregulated upon treatment with AA, which clearly indicates restoration of insulin signaling at transcriptional to the translational level. However, these findings support the relative protein expressions, highlighted by the suppression of insulin signaling by TLR-4 and canonical Wnt pathway in pancreas during T2DM.

In the present work, AA showed promising effect by ameliorating T2DM in subacute disease model of type 2 diabetes by exposing short-term treatment efficacy. Nevertheless, these findings need to be replicated in a long-term chronic disease model of type 2 diabetes with multiple dose testing at cellular level, to further elucidate effects of AA on mitochondrial dysfunction and ER stress during T2DM. Evaluation with multiple dosage would be an important strategy to characterize pharmacokinetic (PK) and pharmacodynamic (PD) movement with regards to concentration and time.

Additionally, PK/PD modeling would establish the chance to understand mechanism of action by identifying PK properties that would enhance AA optimal design on translational platform to study progressive stages in diabetes at clinical level. Effective and successful PK/PD studies might establish AA as a potential drug candidate in the discovery and development process. Further, preclinical studies on small cohort of type 2 diabetic patients would be a good initiative to approach clinical trials on AA.

Conclusion

The current pharmacological investigation revealed potential antidiabetic effects of AA in diabetic rats by mediating through TLR-4 and canonical Wnt/ β -catenin pathway. These findings highlight the lethal crosstalk between TLR-4, Wnt and insulin signaling that

significantly reduced elevated protein and mRNA expression of TLR-4/MyD88 and Wnt/ β -catenin pathway. Therefore, in the light of these findings we suggest that AA is beneficial in the treatment of T2DM by mitigating meta-inflammation and insulin resistance.

Declaration of Interest

The authors declare that they have no conflict of interest.

Acknowledgements

The present work is funded by Taylors University Flagship Research Grant (TUFR/2017/002/01) under Aging and Quality of life. Part of this research is also funded by East West University Center for Research and Training (EWUCRT), Bangladesh.

579 **References**

- 580 Aamir K, Arya A. Emerging role of mRNA and RNA binding proteins in Diabetes.
581 Transcription and Translation in Health and Disease: Elsevier; 2023. p. 243-53.
- 582 Aamir K, Khan HU, Hossain CF, Afrin MR, Jusuf PR, Waheed I, et al. Arjunolic acid
583 downregulates elevated blood sugar and pro-inflammatory cytokines in streptozotocin (STZ)-
584 nicotinamide induced type 2 diabetic rats. Life Sciences. 2021;120232.
- 585 Aamir K, Khan HU, Hossain CF, Afrin MR, Jusuf PR, Waheed I, et al. Arjunolic acid
586 downregulates elevated blood sugar and pro-inflammatory cytokines in streptozotocin (STZ)-
587 nicotinamide induced type 2 diabetic rats. Life sciences. 2022;289:120232.
- 588 Aamir K, Khan HU, Hossain CF, Afrin MR, Shaik I, Salleh N, et al. Oral toxicity of arjunolic
589 acid on hematological, biochemical and histopathological investigations in female Sprague
590 Dawley rats. PeerJ. 2019a;7:e8045.
- 591 Aamir K, Khan HU, Sethi G, Hossain MA, Arya A. Wnt signaling mediates TLR pathway and
592 promote unrestrained adipogenesis and metaflammation: Therapeutic targets for obesity and
593 type 2 diabetes. Pharmacological Research. 2019b;104602.
- 594 Aamir K, Khan HU, Sethi G, Hossain MA, Arya A. Wnt signaling mediates TLR pathway and
595 promote unrestrained adipogenesis and metaflammation: therapeutic targets for obesity and
596 type 2 diabetes. Pharmacological research. 2020;152:104602.
- 597 Ackers I, Malgor R. Interrelationship of canonical and non-canonical Wnt signalling pathways
598 in chronic metabolic diseases. Diabetes and Vascular Disease Research. 2018;15:3-13.
- 599 Almalki DA, Alghamdi SA, Al-Attar AM. Comparative Study on the Influence of Some
600 Medicinal Plants on Diabetes Induced by Streptozotocin in Male Rats. BioMed research
601 international. 2019;2019.
- 602 Arnold AC, Robertson D. Defective Wnt signaling: a potential contributor to cardiometabolic
603 disease? Diabetes. 2015;64:3342-4.

604 Baffy G. Kupffer cells in non-alcoholic fatty liver disease: the emerging view. *Journal of*
605 *hepatology*. 2009;51:212-23.

606 Bartolome A, Zhu C, Sussel L, Pajvani UB. Notch signaling dynamically regulates adult β cell
607 proliferation and maturity. *The Journal of clinical investigation*. 2019;129:268-80.

608 Billiard F, Karaliota S, Wang B, Stellas D, Serafimidis I, Manousopoulou A, et al. Delta-like
609 Ligand-4-Notch signaling inhibition regulates pancreatic islet function and insulin secretion.
610 *Cell reports*. 2018;22:895-904.

611 Cam ME, Hazar-Yavuz AN, Yildiz S, Ertas B, Adakul BA, Taskin T, et al. The methanolic
612 extract of *Thymus praecox* subsp. *skorpilii* var. *skorpilii* restores glucose homeostasis,
613 ameliorates insulin resistance and improves pancreatic β -cell function on
614 streptozotocin/nicotinamide-induced type 2 diabetic rats. *Journal of ethnopharmacology*.
615 2019;231:29-38.

616 Clayton HW, Osipovich AB, Stancill JS, Schneider JD, Vianna PG, Shanks CM, et al.
617 Pancreatic inflammation redirects acinar to β cell reprogramming. *Cell reports*. 2016;17:2028-
618 41.

619 Cross DA, Alessi DR, Cohen P, Andjelkovich M, Hemmings BA. Inhibition of glycogen
620 synthase kinase-3 by insulin mediated by protein kinase B. *Nature*. 1995;378:785-9.

621 Facundo VA, Rios KA, Medeiros CM, Militão JS, Miranda ALP, Epifanio RdA, et al.
622 Arjunolic acid in the ethanolic extract of *Combretum leprosum* root and its use as a potential
623 multi-functional phytomedicine and drug for neurodegenerative disorders: anti-inflammatory
624 and anticholinesterasic activities. *Journal of the Brazilian Chemical Society*. 2005;16:1309-12.

625 Feng J, Lu S, Ou B, Liu Q, Dai J, Ji C, et al. The Role of JNk Signaling Pathway in Obesity-
626 Driven Insulin Resistance. *Diabetes, metabolic syndrome and obesity: targets and therapy*.
627 2020;13:1399.

628 Frasca D, Blomberg BB. Inflammaging decreases adaptive and innate immune responses in
629 mice and humans. *Biogerontology*. 2016;17:7-19.

630 Frasca D, Blomberg BB, Paganelli R. Aging, obesity, and inflammatory age-related diseases.
631 *Frontiers in immunology*. 2017;8:1745.

632 George MD, Baker JF. The obesity epidemic and consequences for rheumatoid arthritis care.
633 *Current rheumatology reports*. 2016;18:6.

634 Ghosh J, Das J, Manna P, Sil PC. Protective effect of the fruits of *Terminalia arjuna* against
635 cadmium-induced oxidant stress and hepatic cell injury via MAPK activation and mitochondria
636 dependent pathway. *Food chemistry*. 2010;123:1062-75.

637 Guilherme A, Henriques F, Bedard AH, Czech MP. Molecular pathways linking adipose
638 innervation to insulin action in obesity and diabetes mellitus. *Nature Reviews Endocrinology*.
639 2019;15:207-25.

640 Halban PA, Polonsky KS, Bowden DW, Hawkins MA, Ling C, Mather KJ, et al. β -cell failure
641 in type 2 diabetes: postulated mechanisms and prospects for prevention and treatment. *The*
642 *Journal of Clinical Endocrinology & Metabolism*. 2014;99:1983-92.

643 Hameed I, Masoodi SR, Mir SA, Nabi M, Ghazanfar K, Ganai BA. Type 2 diabetes mellitus:
644 from a metabolic disorder to an inflammatory condition. *World journal of diabetes*.
645 2015;6:598.

646 Hotamisligil GS. Inflammation, metaflammation and immunometabolic disorders. *Nature*.
647 2017;542:177.

648 Hussien NI, Ebrahim N, Mohammed OM, Sabry D. Combination of obestatin and bone marrow
649 mesenchymal stem cells prevents aggravation of endocrine pancreatic damage in type II
650 diabetic rats. *International journal of stem cells*. 2017;10:129.

651 Khan HU, Aamir K, Jusuf PR, Sethi G, Sisinthy SP, Ghildyal R, et al. Lauric acid ameliorates
 652 lipopolysaccharide (LPS)-induced liver inflammation by mediating TLR4/MyD88 pathway in
 653 Sprague Dawley (SD) rats. *Life Sciences*. 2020;118750.
 654 Lanuza-Masdeu J, Arévalo MI, Vila C, Barberà A, Gomis R, Caelles C. In vivo JNK activation
 655 in pancreatic β -cells leads to glucose intolerance caused by insulin resistance in pancreas.
 656 *Diabetes*. 2013;62:2308-17.
 657 Li M, Song L, Gao X, Chang W, Qin X. Toll-like receptor 4 on islet β cells senses expression
 658 changes in high-mobility group box 1 and contributes to the initiation of type 1 diabetes.
 659 *Experimental & molecular medicine*. 2012;44:260-7.
 660 Ma B, Hottiger MO. Crosstalk between Wnt/ β -catenin and NF- κ B signaling pathway during
 661 inflammation. *Frontiers in immunology*. 2016;7:378.
 662 Manna P, Das J, Ghosh J, Sil PC. Contribution of type 1 diabetes to rat liver dysfunction and
 663 cellular damage via activation of NOS, PARP, I κ B α /NF- κ B, MAPKs, and mitochondria-
 664 dependent pathways: prophylactic role of arjunolic acid. *Free Radical Biology and Medicine*.
 665 2010;48:1465-84.
 666 Manna P, Sil PC. Arjunolic acid: beneficial role in type 1 diabetes and its associated organ
 667 pathophysiology. *Free radical research*. 2012;46:815-30.
 668 Marchese D, de Groot NS, Lorenzo Gotor N, Livi CM, Tartaglia GG. Advances in the
 669 characterization of RNA-binding proteins. *Wiley Interdisciplinary Reviews: RNA*.
 670 2016;7:793-810.
 671 Mega C, Vala H, Rodrigues-Santos P, Oliveira J, Teixeira F, Fernandes R, et al. Sitagliptin
 672 prevents aggravation of endocrine and exocrine pancreatic damage in the Zucker Diabetic Fatty
 673 rat-focus on amelioration of metabolic profile and tissue cytoprotective properties. *Diabetology*
 674 & metabolic syndrome. 2014;6:42.

675 Nie X, Wei X, Ma H, Fan L, Chen WD. The complex role of Wnt ligands in type 2 diabetes
 676 mellitus and related complications. *Journal of Cellular and Molecular Medicine*.
 677 2021;25:6479-95.

678 Nolan CJ, Damm P, Prentki M. Type 2 diabetes across generations: from pathophysiology to
 679 prevention and management. *The Lancet*. 2011;378:169-81.

680 Noor A, Gunasekaran S, Vijayalakshmi M. Improvement of insulin secretion and pancreatic
 681 β -cell function in streptozotocin-induced diabetic rats treated with Aloe vera extract.
 682 *Pharmacognosy research*. 2017;9:S99.

683 Ottaviani S, Allanore Y, Tubach F, Forien M, Gardette A, Pasquet B, et al. Body mass index
 684 influences the response to infliximab in ankylosing spondylitis. *Arthritis research & therapy*.
 685 2012;14:R115.

686 Radziszewska A, Schroer SA, Choi D, Tajmir P, Radulovich N, Ho JC, et al. Absence of
 687 caspase-3 protects pancreatic β -cells from c-Myc-induced apoptosis without leading to tumor
 688 formation. *Journal of Biological Chemistry*. 2009;284:10947-56.

689 Scheibner K, Bakhti M, Bastidas-Ponce A, Lickert H. Wnt signaling: implications in endoderm
 690 development and pancreas organogenesis. *Current Opinion in Cell Biology*. 2019;61:48-55.

691 Shi H, Kokoeva MV, Inouye K, Tzameli I, Yin H, Flier JS. TLR4 links innate immunity and
 692 fatty acid-induced insulin resistance. *The Journal of clinical investigation*. 2006;116:3015-25.

693 Singh A, Kukal S, Kanojia N, Singh M, Saso L, Kukreti S, et al. Lipid Mediated Brain
 694 Disorders: A Perspective. *Prostaglandins & Other Lipid Mediators*. 2023:106737.

695 Singh A, Kukreti R, Saso L, Kukreti S. Mechanistic insight into oxidative stress-triggered
 696 signaling pathways and type 2 diabetes. *Molecules*. 2022;27:950.

697 Xu X, Liang T, Lin X, Wen Q, Liang X, Li W, et al. Effect of the total extract of
 698 *Averrhoacarambola* (oxalidaceae) root on the expression levels of TLR4 and NF- κ B in

streptozotocin-induced diabetic mice. Cellular Physiology and Biochemistry. 2015;36:2307-16.

Yang Y, Lv J, Jiang S, Ma Z, Wang D, Hu W, et al. The emerging role of Toll-like receptor 4 in myocardial inflammation. Cell death & disease. 2016;7:e2234-e.

Yung JHM, Giacca A. Role of c-Jun N-terminal kinase (JNK) in obesity and type 2 diabetes. Cells. 2020;9:706.

Zhou J, Zhou S, Zeng S. Experimental diabetes treated with trigonelline: effect on β cell and pancreatic oxidative parameters. Fundamental & clinical pharmacology. 2013;27:279-87.

Figure 1. Photomicrographs of H&E stained pancreas of different groups. (A) Normal control displayed granulated cytoplasm, islets with large nuclei (beta-cells) (arrowhead) and small dark nuclei present in periphery (alpha-cells) (arrow). Exocrine portion represent regular shape of acinar cells (broad arrow). (B) Non-treated diabetic rats showed shrunk islets with reduced size and number, vacuolated cytoplasm (circle), congested blood vessels (arrow with box-head) and karyolysis. (C) Treatment with low dose AA presented increment in cell number with slight improvement in shape. Few islets still exhibit darkly stained nuclei and vacuolated cytoplasm, however slight restoration in shape of acinar cells. (D) Treatment with high dose of AA exhibited marked improvement in shape and number of islets (alpha and beta cells) and acinar cells. (E) Metformin treatment further improved overall histoarchitecture and cytology. NC normal control; DC diabetic control; ALD arjunolic acid low dose; AHD arjunolic acid high dose; MET metformin (H&E stain x200).

Figure 2. Photomicrographs of Masson trichrome stained pancreas sections of different groups. (A). Normal control showed regular tissue architecture with proper outlined alpha (arrow) and beta cells (arrowhead). (B). Diabetic rats displayed shrunk, pyknotic nuclei with drastic decrease in islets size and number, distorted shape of pancreatic acini (broad arrow) and deposition of collagen fiber (rectangle). (C). Treatment with 25 mg/kg AA increase cell size and number with reduction in collagen deposition. (D). Treatment with 50 mg/kg AA completely abolished collagen stroma with nearly regular outline of islets. (E). Treatment with metformin (250 mg/kg) improved islets shape and number as compared to diabetic control. NC normal control; DC diabetic control; ALD arjunolic acid low dose; AHD arjunolic acid high dose; MET metformin (MT stain x200).

Figure 3. Histomorphometric analysis of H&E stained pancreas of different groups. (A) Normal control displayed regular morphology and size of islets. (B) Non-treated diabetic rats showed shrunk islets with reduced size (arrow) and congested blood vessels (broad arrow). (C) Treatment with low dose AA presented increase in cell number with slight improvement in shape. Few islets still exhibit disorganized shape (arrow) and congested blood vessel (broad arrow). (D) Treatment with high dose of AA exhibited considerable improvement in shape, size and number of islets (arrow). (E) Metformin treatment displayed near to normal islets shape and size. (F) Graphical presentation of islets size from control and treated groups. NC normal control; DC diabetic control; ALD arjunolic acid low dose; AHD arjunolic acid high dose; MET metformin (H&E stain x400). Non-significant (ns), $*p<0.05$, $**p<0.005$ when compared with DC.

Figure 4. Jess analysis showing expression of TLR-4 in pancreas of control and treated groups. (A) Protein normalization. (B) Band density representing expression of TLR-4 in normal, diabetic and treated groups. (C) Gradual peaks presenting AUC for expression of TLR-4. (D) Graph plotted between groups and AUC presenting statistical analysis for the expression of TLR-4. NC normal control; DC diabetic control; ALD arjunolic acid low dose; AHD arjunolic acid high dose; MET metformin; AUC area under curve. Non-significant (ns) when compared with DC.

Figure 5. Jess analysis presenting expression of MyD88 in pancreas of control and treated groups. (A) Protein normalization. (B) Band density representing expression of MyD88 in normal, diabetic and treated groups. (C) Gradual peaks presenting AUC for expression of MyD88. (D) Graph plotted between groups and AUC presenting statistical analysis for the expression of MyD88. NC normal control; DC diabetic control; ALD arjunolic acid low dose; AHD arjunolic acid high dose; MET metformin; AUC area under curve. Non-significant (ns), $*p<0.05$, $**p<0.005$, $***p<0.001$ when compared with DC.

Figure 6. Jess analysis presenting expression of NF- κ B in pancreas of control and treated groups. (A) Protein normalization. (B) Band density representing expression of NF- κ B in normal, diabetic and treated groups. (C) Gradual peaks presenting AUC for expression of NF- κ B. (D) Graph plotted between groups and AUC presenting statistical analysis for the expression of NF- κ B. NC normal control; DC diabetic control; ALD arjunolic acid low dose; AHD arjunolic acid high dose; MET metformin; AUC area under curve. $**p<0.005$ when compared with DC.

Figure 7. Jess analysis showing expression of p-JNK1/2 in pancreas of control and treated groups. (A) Protein normalization. (B) Band density representing expression of p-JNK1/2 in normal, diabetic and treated groups. (C) Gradual peaks presenting AUC for expression of p-JNK1/2. (D) Graph plotted between groups and AUC presenting statistical analysis for the expression of p-JNK1/2. NC normal control; DC diabetic control; ALD arjunolic acid low dose; AHD arjunolic acid high dose; MET metformin; AUC area under curve. $**p<0.005$, $***p<0.001$ when compared with DC.

Figure 8. Jess analysis showing expression of IRS-1 in pancreas of control and treated groups. (A) Protein normalization. (B) Band density representing expression of IRS-1 in normal, diabetic and treated groups. (C) Gradual peaks presenting AUC for expression of IRS-1. (D) Graph plotted between groups and AUC presenting

statistical analysis for the expression of IRS-1. NC normal control; DC diabetic control; ALD arjunolic acid low dose; AHD arjunolic acid high dose; MET metformin; AUC area under curve. Non-significant (ns), **** $p<0.0001$ when compared with DC.

Figure 9. Jess analysis showing expression of PI3K in pancreas of control and treated groups. (A) Protein normalization. (B) Band density representing expression of PI3K in normal, diabetic and treated groups. (C) Gradual peaks presenting AUC for expression of PI3K. (D) Graph plotted between groups and AUC presenting statistical analysis for the expression of PI3K. NC normal control; DC diabetic control; ALD arjunolic acid low dose; AHD arjunolic acid high dose; MET metformin; AUC area under curve. Non-significant (ns), ** $p<0.005$ when compared with DC.

Figure 10. Jess analysis showing expression of p-Akt1/2/3 in pancreas of control and treated groups. (A) Protein normalization. (B) Band density representing expression of p-Akt1/2/3 in normal, diabetic and treated groups. (C) Gradual peaks presenting AUC for expression of p-Akt1/2/3. (D) Graph plotted between groups and AUC presenting statistical analysis for the expression of p-Akt1/2/3. NC normal control; DC diabetic control; ALD arjunolic acid low dose; AHD arjunolic acid high dose; MET metformin; AUC area under curve. Non-significant (ns), * $p<0.05$ when compared with DC.

Figure 11. Jess analysis showing expression of Wnt3a in pancreas of control and treated groups. (A) Protein normalization. (B) Band density representing expression of Wnt3a in normal, diabetic and treated groups. (C) Gradual peaks presenting AUC for expression of Wnt3a. (D) Graph plotted between groups and AUC presenting statistical analysis for the expression of Wnt3a. NC normal control; DC diabetic control; ALD arjunolic acid low dose; AHD arjunolic acid high dose; MET metformin; AUC area under curve. *** $p<0.001$ when compared with DC.

Figure 12. Jess analysis showing expression of β -catenin in pancreas of control and treated groups. (A) Protein normalization. (B) Band density representing expression of β -catenin in normal, diabetic and treated groups. (C) Gradual peaks presenting AUC for expression of β -catenin. (D) Graph plotted between groups and AUC presenting statistical analysis for the expression of β -catenin. NC normal control; DC diabetic control; ALD arjunolic acid low dose; AHD arjunolic acid high dose; MET metformin; AUC area under curve. Non-significant (ns), * $p<0.05$, ** $p<0.005$ when compared with DC.

Figure 13. Jess analysis showing expression of c-Myc in pancreas of control and treated groups. (A) Protein normalization. (B) Band density representing expression of c-Myc in normal, diabetic and treated groups. (C) Gradual peaks presenting AUC for expression of c-Myc. (D) Graph plotted between groups and AUC presenting statistical analysis for the expression of c-Myc. NC normal control; DC diabetic control; ALD arjunolic acid low dose; AHD arjunolic acid high dose; MET metformin; AUC area under curve. Non-significant (ns), * $p<0.05$ when compared with DC.

Figure 14. Heatmap showing protein expression of selected protein targets from pancreas of control and treated groups. NC normal control; DC diabetic control; ALD arjunolic acid low dose; AHD arjunolic acid high dose; MET metformin.

Figure 15. Representative immunohistochemistry images showing TLR-4 localization in pancreas as indicated by dark brown staining along with graphical presentation demonstrating AUC for expression of TLR-4 in control and treated groups. NC normal control; DC diabetic control; ALD arjunolic acid low dose; AHD arjunolic acid high dose; MET metformin; AUC area under curve. **** $p<0.0001$ when compared with DC.

Figure 16. Representative immunohistochemistry images showing MyD88 localization in pancreas as indicated by dark brown staining along with graphical presentation demonstrating AUC for expression of MyD88 in control and treated groups. NC normal control; DC diabetic control; ALD arjunolic acid low dose; AHD arjunolic acid high dose; MET metformin; AUC area under curve. Non-significant (ns), ** $p<0.005$ when compared with DC.

Figure 17. Representative immunohistochemistry images showing NF- κ B localization in pancreas as indicated by dark brown staining along with graphical presentation demonstrating AUC for expression of NF- κ B in control and treated groups. NC normal control; DC diabetic control; ALD arjunolic acid low dose; AHD arjunolic acid high dose; MET metformin; AUC area under curve. *** $p<0.001$, **** $p<0.0001$ when compared with DC.

Figure 18. Representative immunohistochemistry images showing p-JNK1/2 localization in pancreas as indicated by dark brown staining along with graphical presentation demonstrating AUC for expression of p-JNK1/2 in

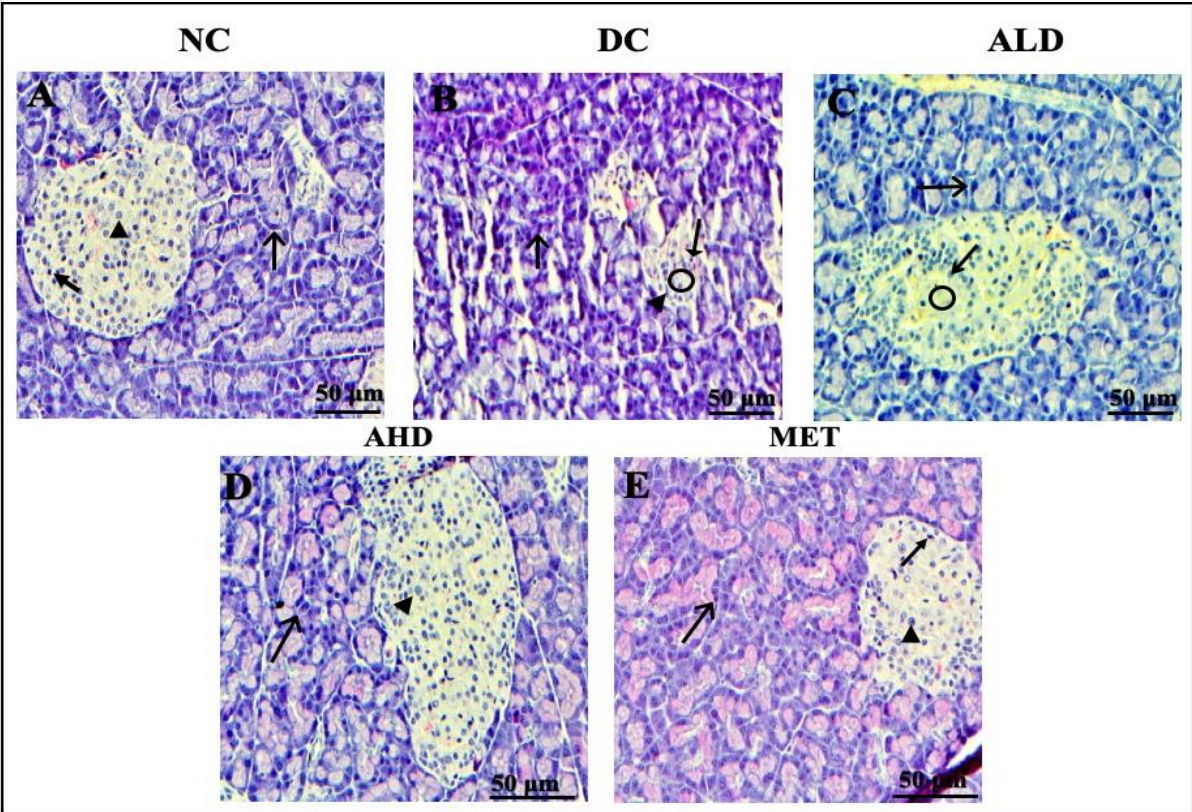
control and treated groups. NC normal control; DC diabetic control; ALD arjunolic acid low dose; AHD arjunolic acid high dose; MET metformin; AUC area under curve. **** $p<0.0001$ when compared with DC.

Figure 19. Representative immunohistochemistry images showing IRS-1 localization in pancreas as indicated by dark brown staining along with graphical presentation demonstrating AUC for expression of IRS-1 in control and treated groups. NC normal control; DC diabetic control; ALD arjunolic acid low dose; AHD arjunolic acid high dose; MET metformin; AUC area under curve. Non-significant (ns), ** $p<0.005$, *** $p<0.001$, **** $p<0.0001$ when compared with DC.

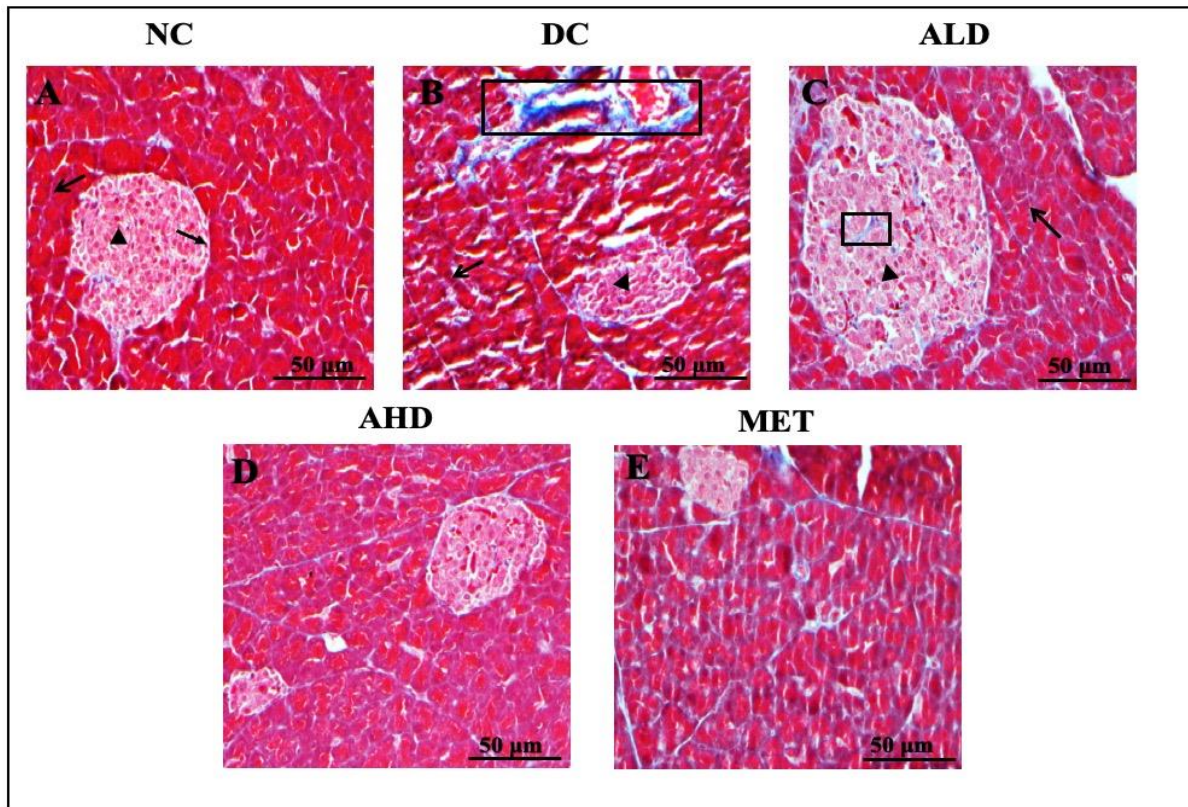
Figure 20. Representative immunohistochemistry images showing Wnt3a localization in pancreas as indicated by dark brown staining along with graphical presentation demonstrating AUC for expression of Wnt3a in control and treated groups. NC normal control; DC diabetic control; ALD arjunolic acid low dose; AHD arjunolic acid high dose; MET metformin; AUC area under curve. Non-significant (ns), **** $p<0.0001$ when compared with DC.

Figure 21. Representative immunohistochemistry images showing β -catenin localization in pancreas as indicated by dark brown staining along with graphical presentation demonstrating AUC for expression of β -catenin in control and treated groups. NC normal control; DC diabetic control; ALD arjunolic acid low dose; AHD arjunolic acid high dose; MET metformin; AUC area under curve. **** $p<0.0001$ when compared with DC.

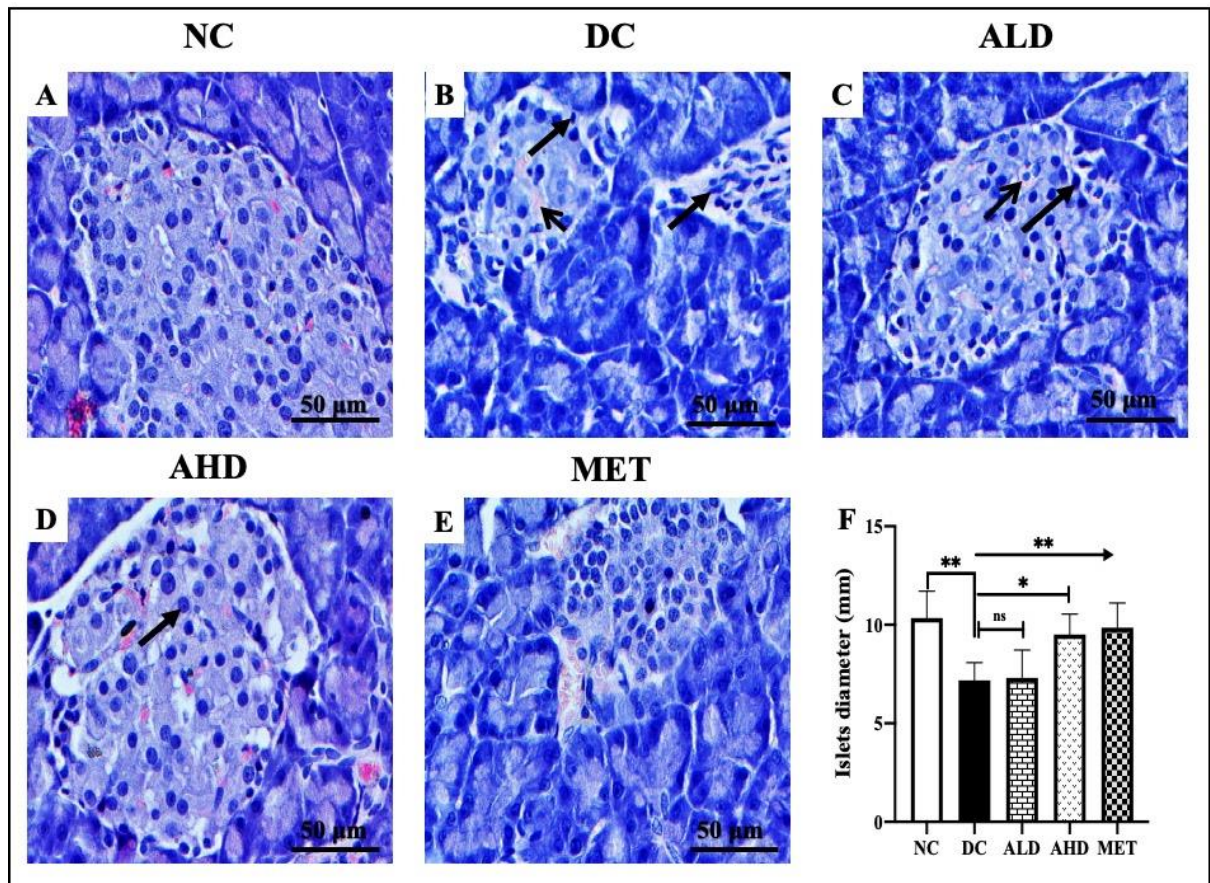
Figure 22. Graphs presenting mRNA expression of TLR-4, MyD88, NF- κ B, TNF- α , IL-1 β , IRS-1, Wnt3a, β -catenin and c-Myc in pancreas of control and treated groups. NC normal control; DC diabetic control; ALD arjunolic acid low dose; AHD arjunolic acid high dose; MET metformin. Non-significant (ns), * $p<0.05$, ** $p<0.005$, *** $p<0.001$ when compared with DC.



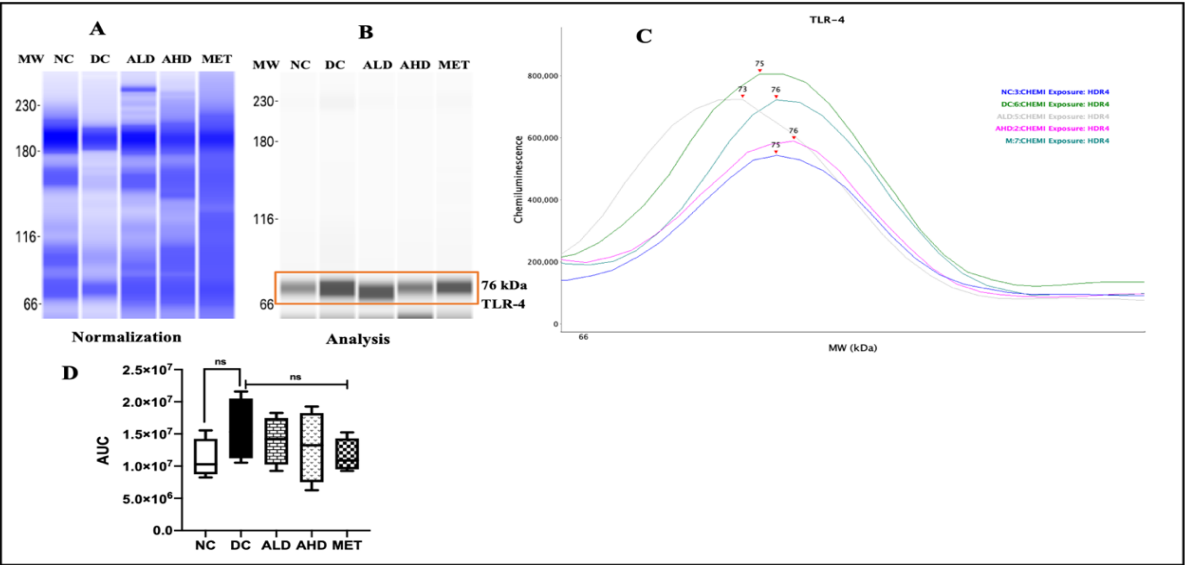
902
903
904
905
906
907
908
909
910
911
912
913
914
915
916
917
918
919
920
921
922
923
924
925
926
927
928
929
930
931

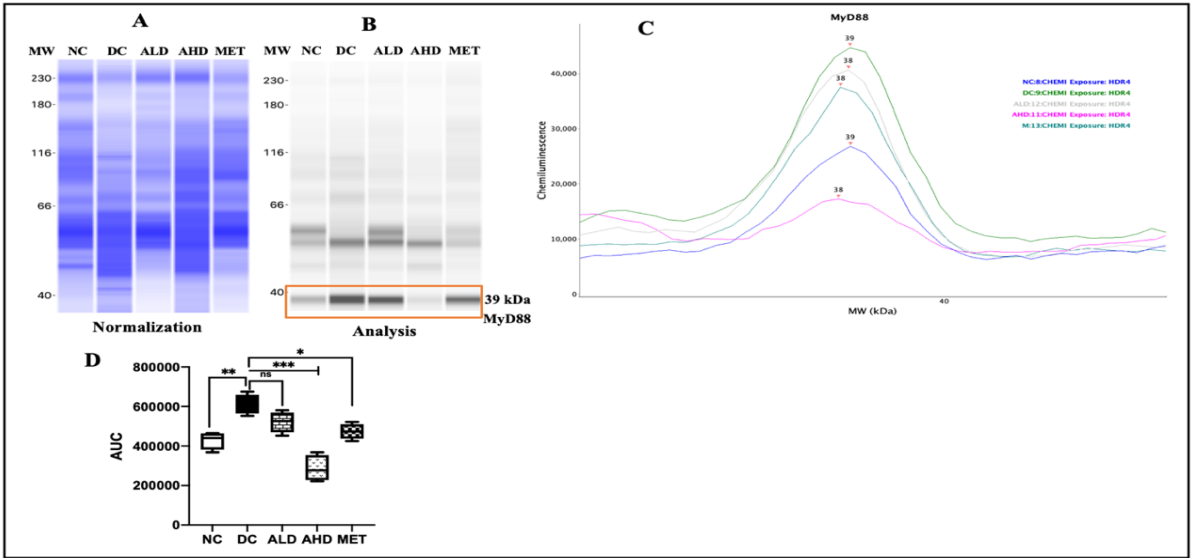


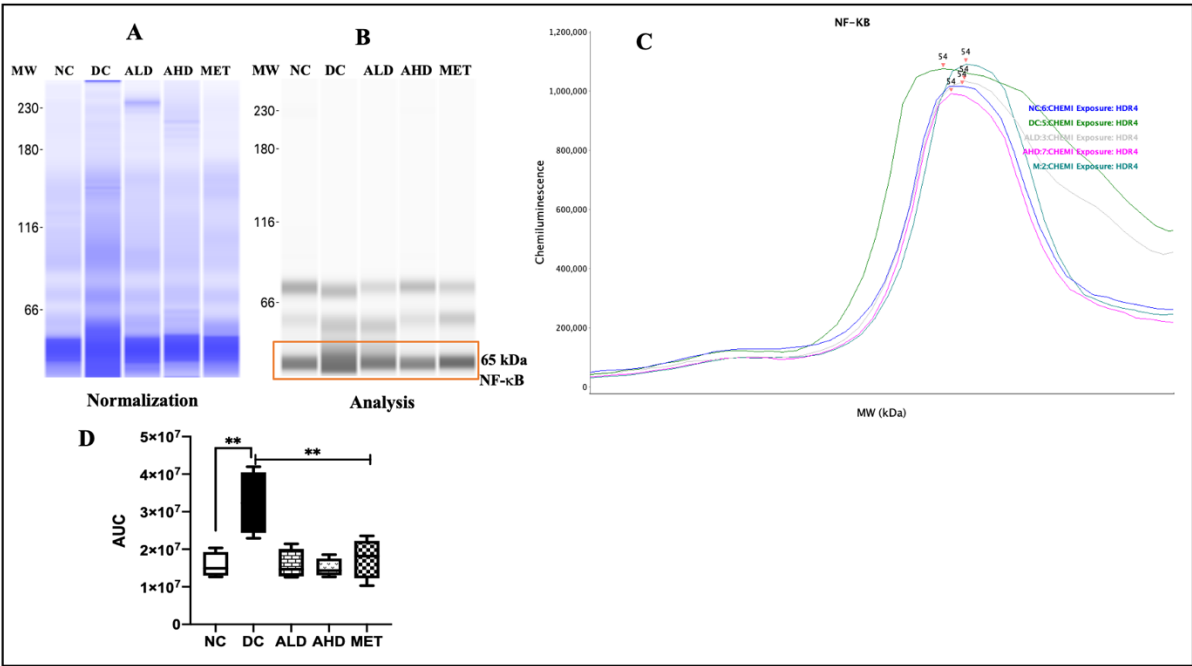
932
933
934
935
936
937
938
939
940
941
942
943
944
945
946
947
948
949
950
951
952
953
954
955
956
957
958
959
960

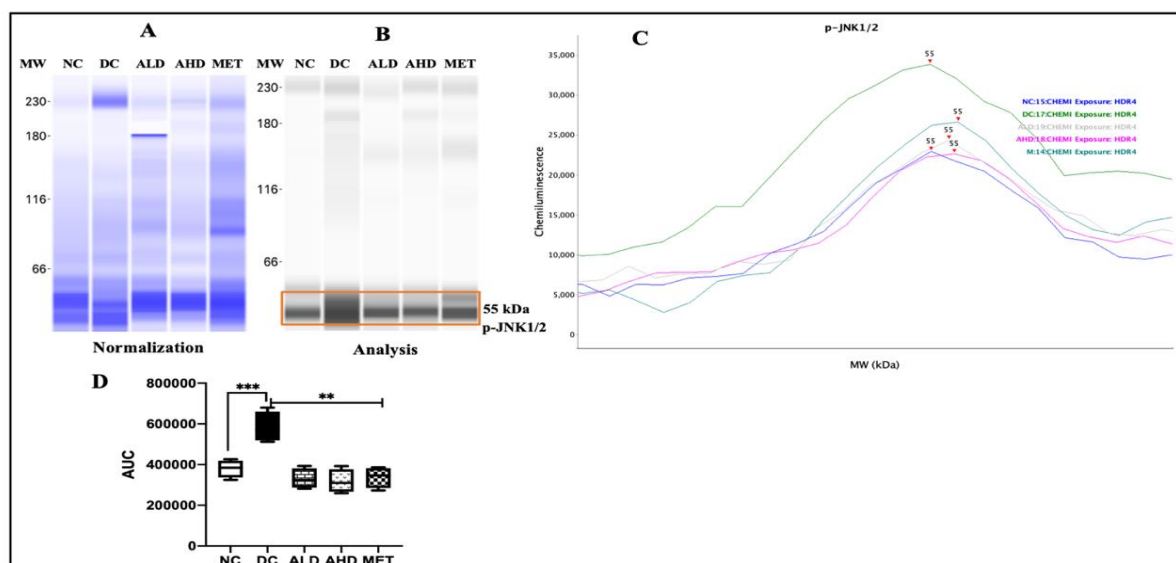


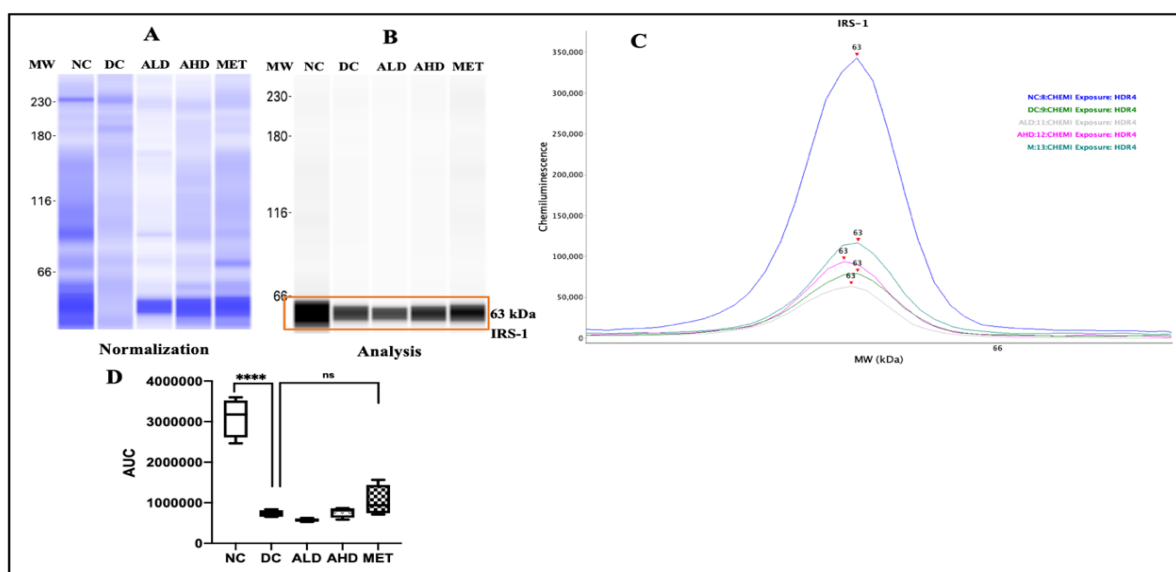
961
962
963
964
965
966
967
968
969
970
971
972
973
974
975
976
977
978
979
980
981
982
983
984
985
986
987

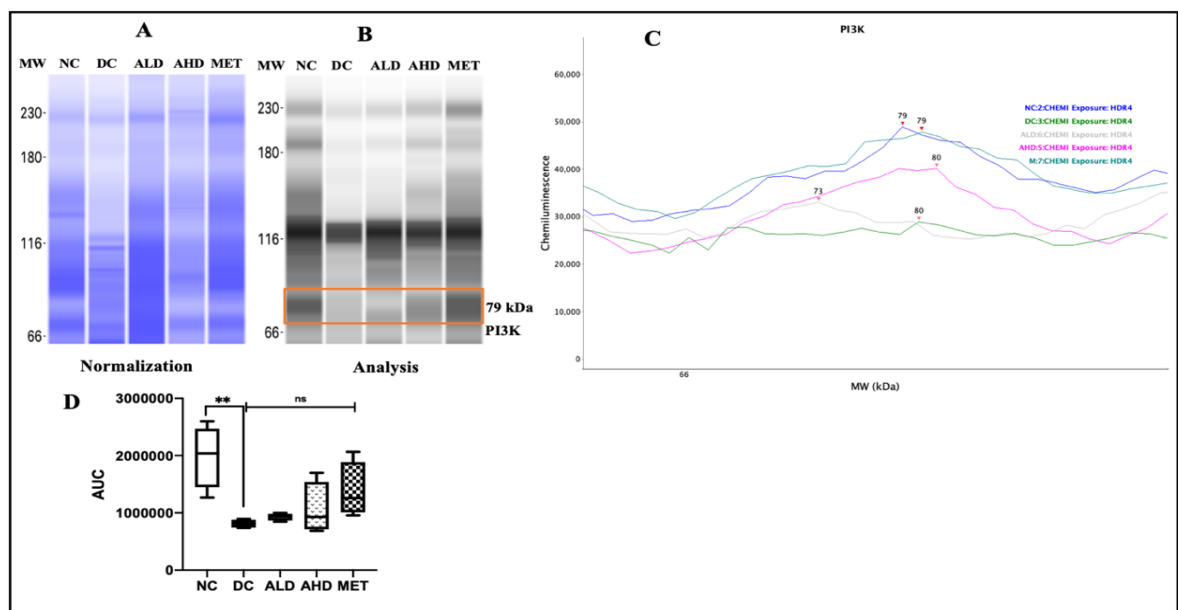




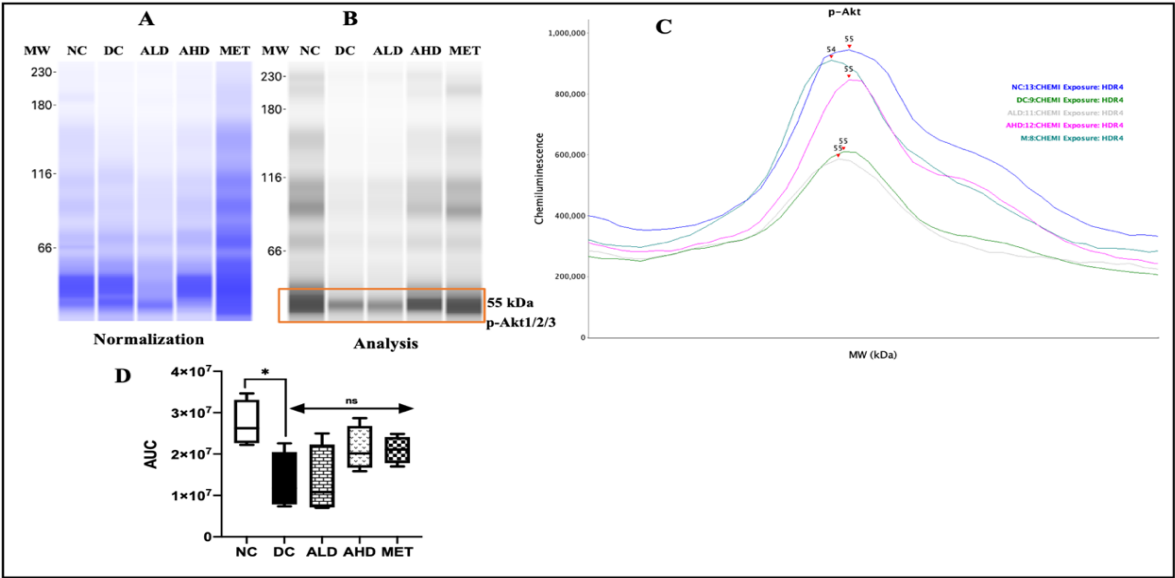




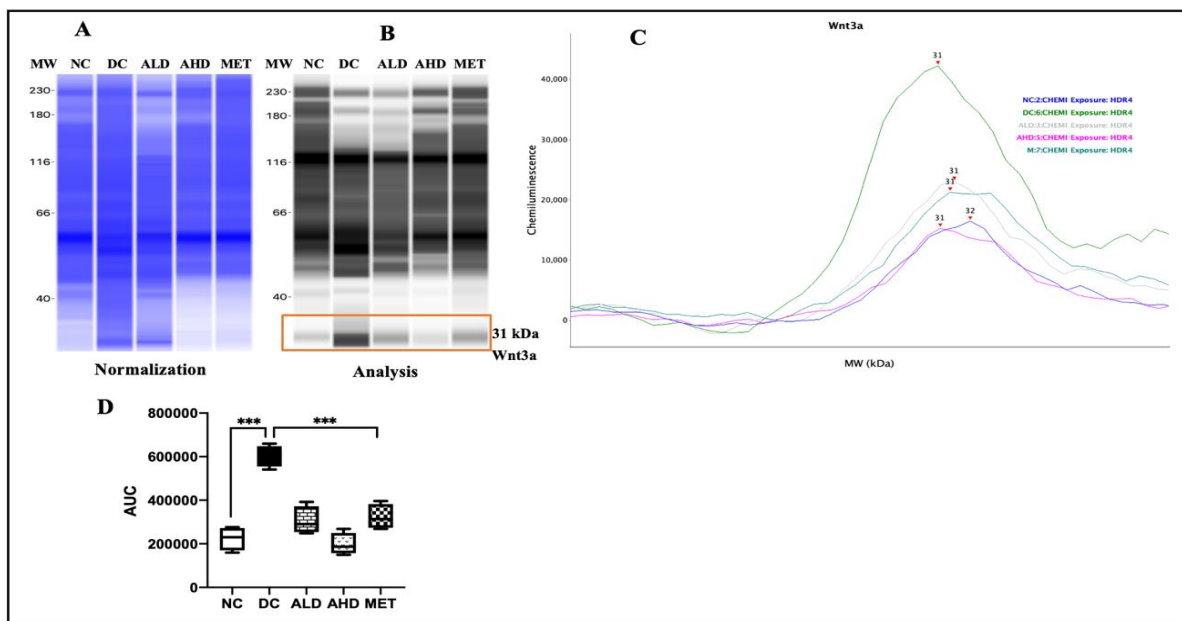


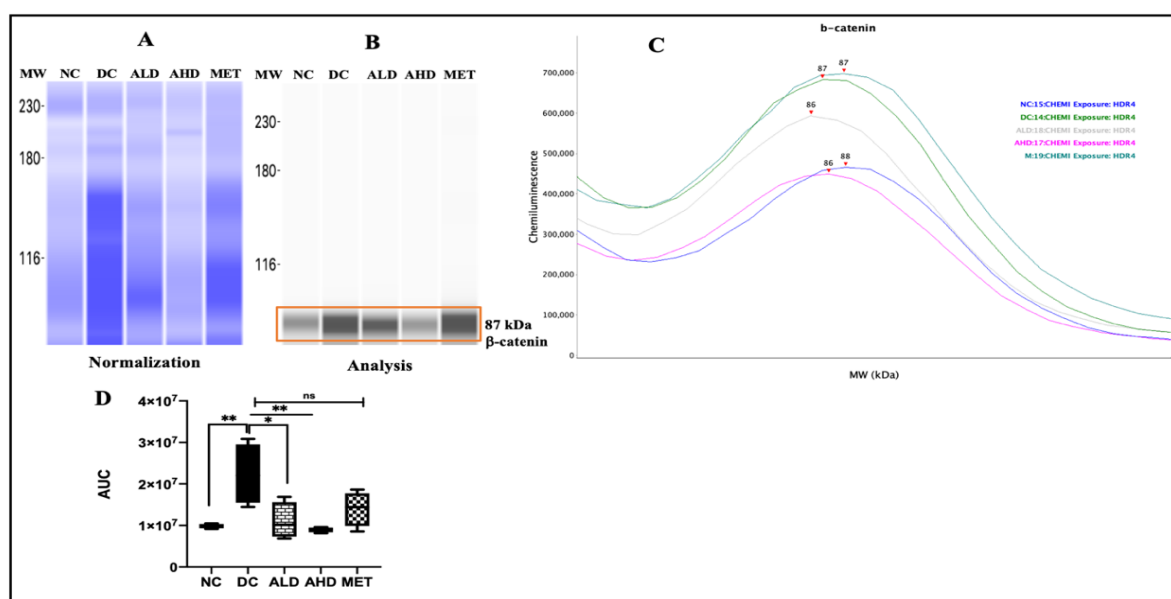


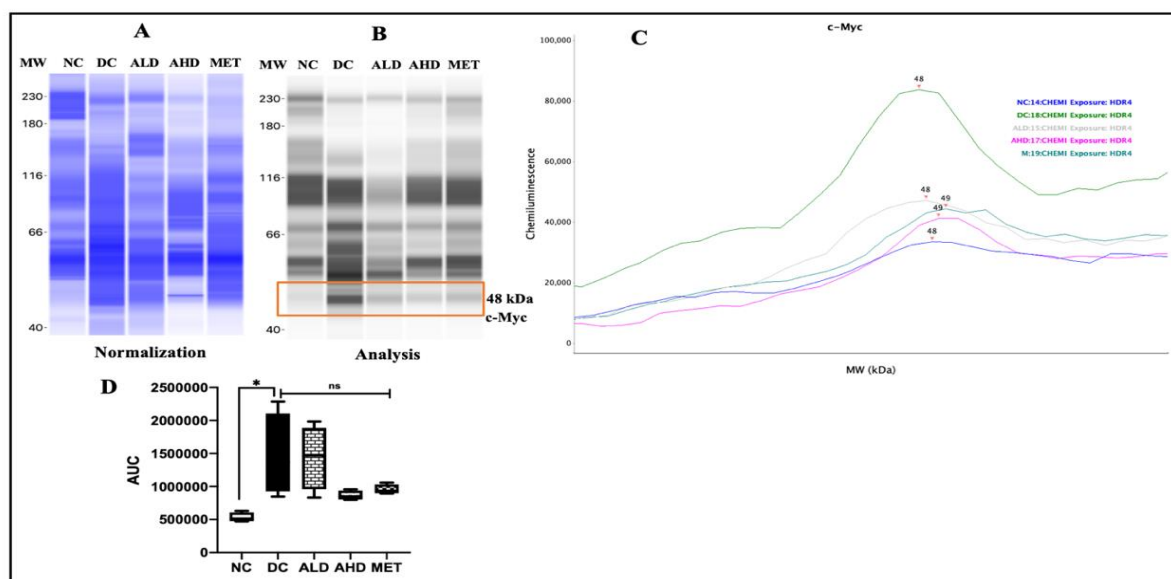
1196

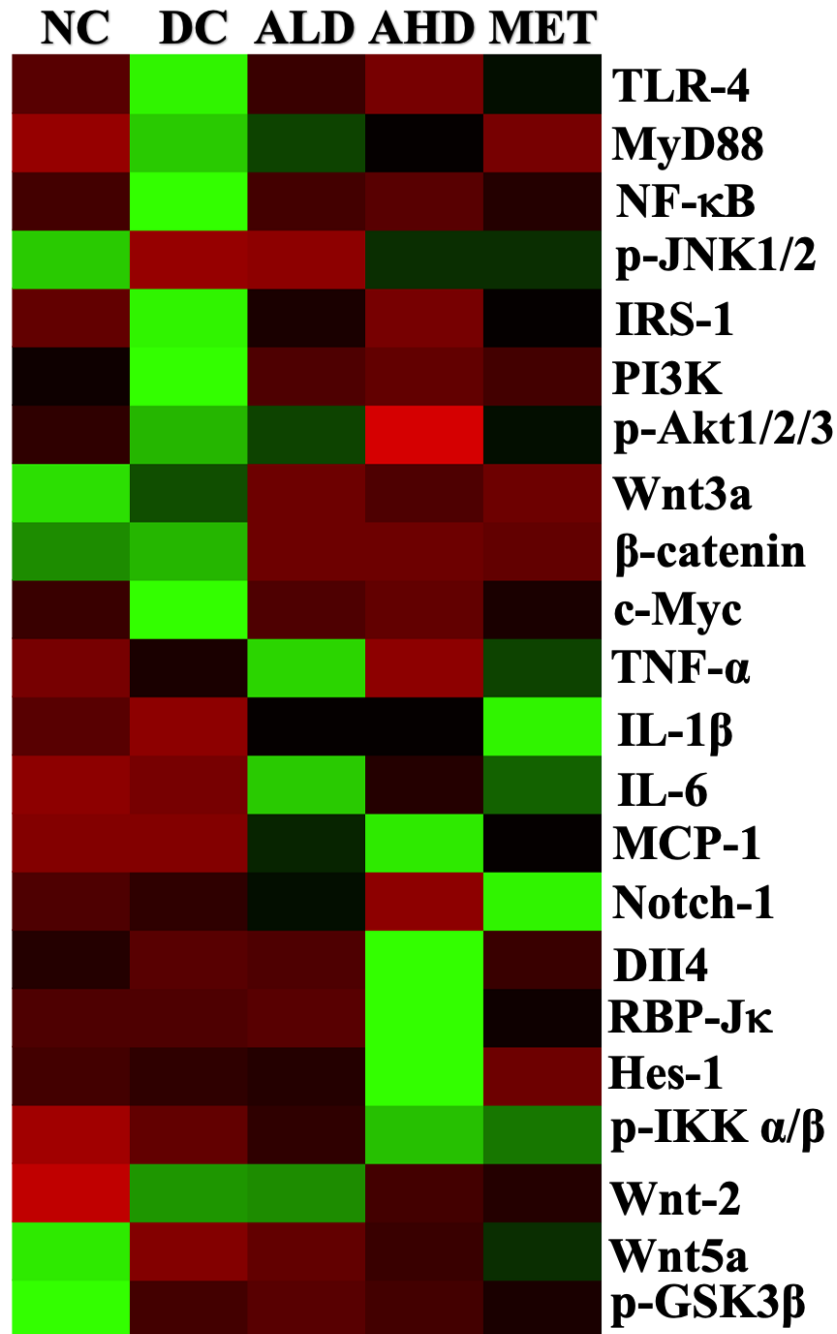
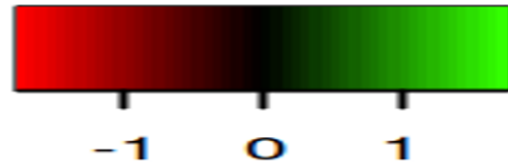


1197
1198
1199
1200
1201
1202
1203
1204
1205
1206
1207
1208
1209
1210
1211
1212
1213
1214
1215
1216
1217
1218
1219
1220
1221
1222
1223
1224
1225
1226
1227
1228
1229
1230

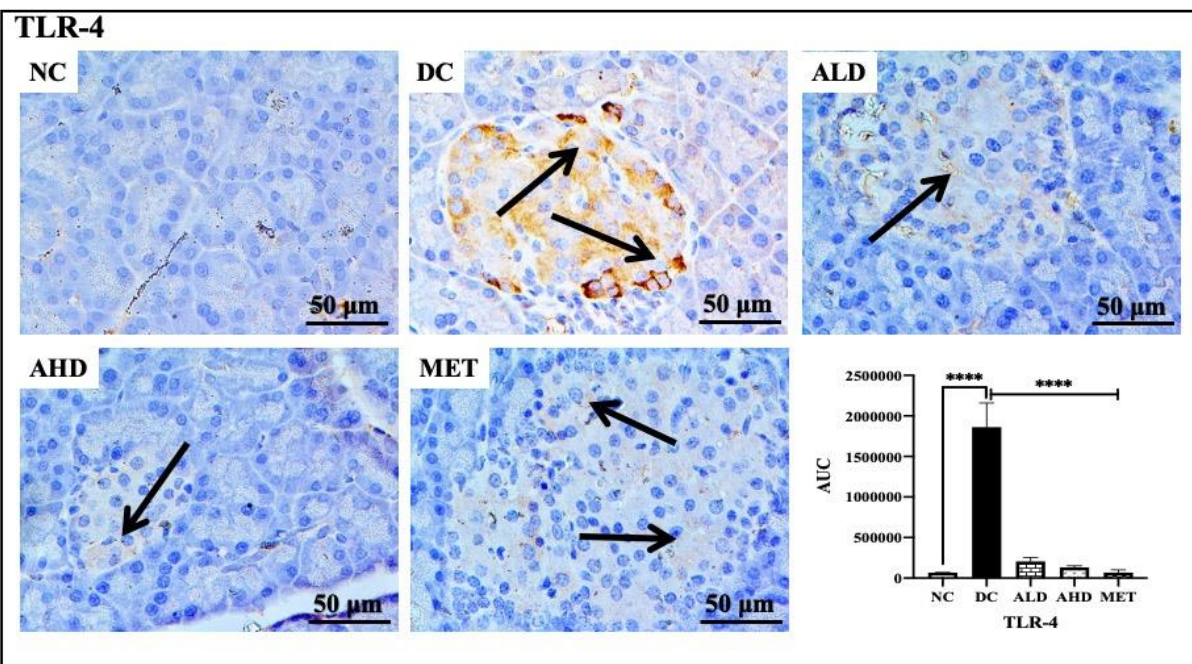


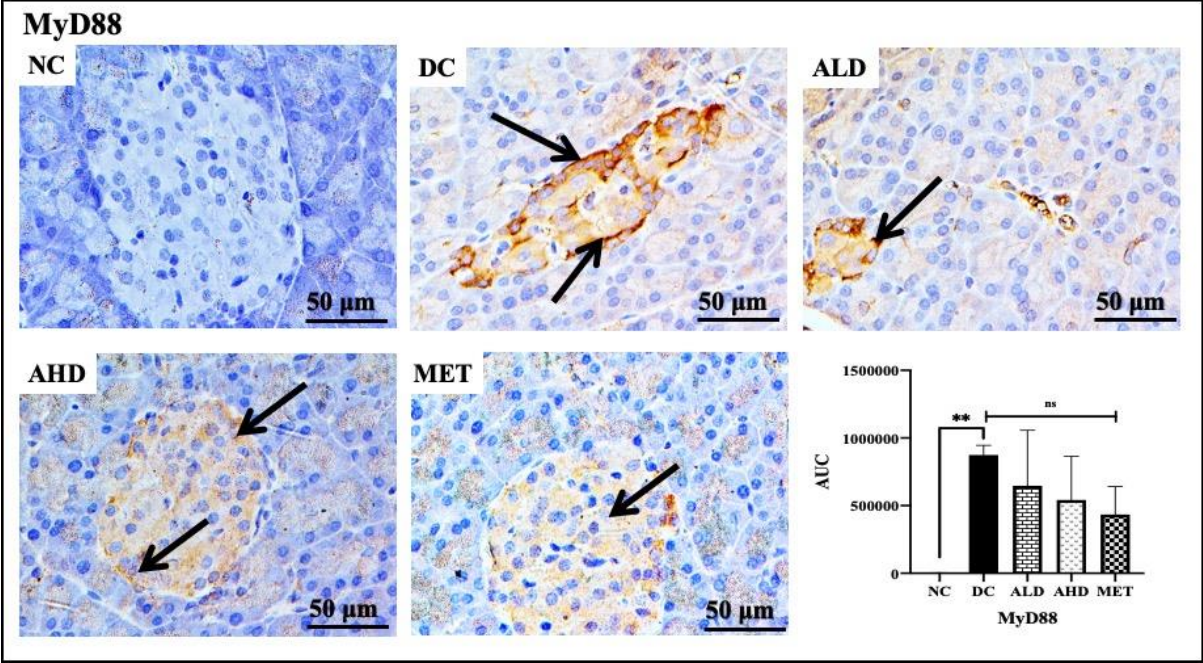




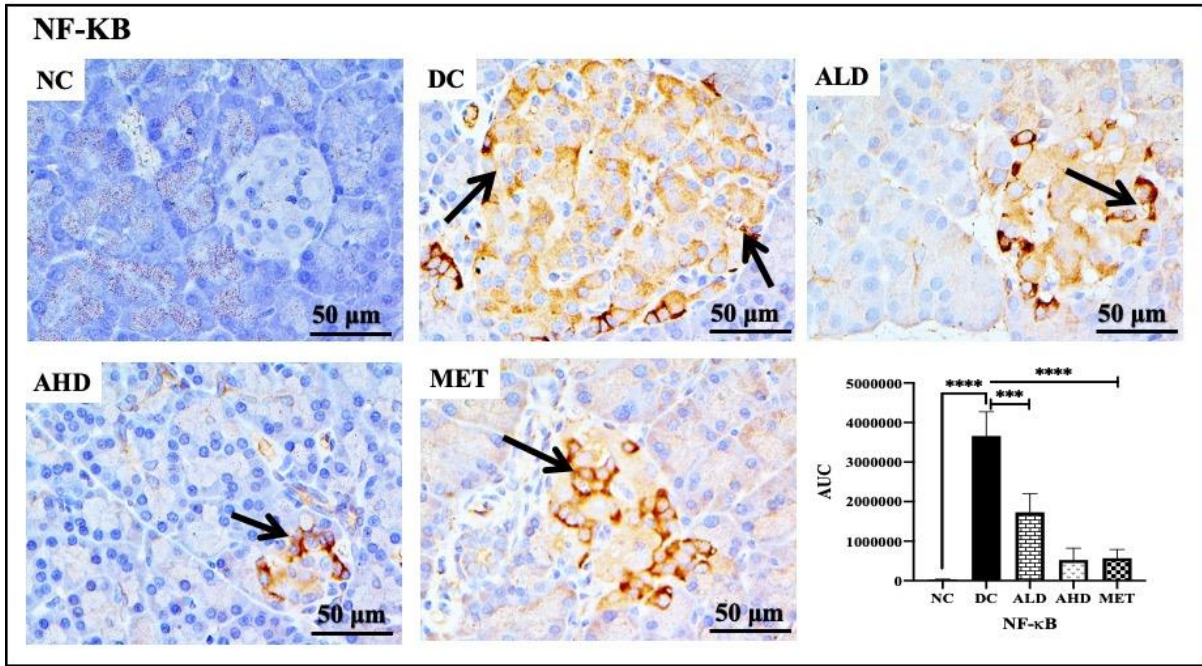


1334
1335
1336
1337
1338
1339
1340





1374
1375
1376
1377
1378
1379
1380
1381
1382
1383
1384
1385
1386
1387
1388
1389
1390
1391
1392
1393
1394
1395
1396
1397
1398
1399
1400



1401
1402
1403
1404
1405
1406
1407
1408
1409
1410
1411
1412
1413
1414
1415
1416
1417
1418
1419
1420
1421
1422
1423
1424
1425
1426
1427
1428
1429
1430
1431
1432
1433

